Rheological Properties of $MgSiO_3$ Perovskite and Its Implications for the Lower Mantle

$MgSiO_3$ペロブスカイトと下部マントルのレオロジー

山崎大輔

学位論文

Rheological Properties of $MgSiO_3$ Perovskite and Its Implications for the Lower Mantle

$MgSiO_3$ペロブスカイトと下部マントルのレオロジー

平成9年12月博士(理学)申請

東京大学大学院理学系研究科
地質学専攻

山崎 大輔

Abstract

Earth's lower mantle is mainly composed of $(Mg,Fe)SiO_3$ perovskite and (Mg,Fe)O magnesiowüstite. It is essential to determine the rheological properties of $MgSiO_3$ perovskite and periclase for understanding the rheology of the lower mantle. Determination of diffusion coefficients and estimation of grain size of constituent materials are the most important parameter among the rheological properties, because dominant deformation mechanism in the lower mantle is considered to be diffusion creep.

Mg_2SiO_4 spinel transform to $MgSiO_3$ perovskite and periclase by the incoherent and nucleation and growth mechanism based on the TEM examination. The grain growth rates of $MgSiO_3$ perovskite and periclase in aggregates have been determined at 25 gigapascals and 1573 to 2173 kelvin. The average grain size (G) was fitted to the rate equation, and the grain growth rates of perovskite and periclase were $G^{10.6}=1 \times 10^{-57.4} t \exp(-320.8/RT)$ and $G^{10.8}=1 \times 10^{-62.3} t \exp(-247.0/RT)$, respectively, where t is the time, R is the gas constant and T is the absolute temperature. On the other hand, the grain growth rate of $MgSiO_3$ perovskite single phase was obtained to be $G^{5.3}=10^{-33.3}t$ at constant temperature of 1873 K. The lattice diffusion coefficient (D_l) and grain boundary diffusion coefficient (D_{gb}) of silicon in $MgSiO_3$ perovskite were determined to be $D_l=4.12\times10^{-10}\exp(-341/RT)$ and $\delta D_{gb}=1.88\times10^{-16}\exp(-310/RT)$, respectively, at pressure of 25 GPa and temperature range of 1673-2073 K, where δ is the width of the grain boundary.

Consequently, it can be estimate that the viscosity of the subducted slab is 10^{17}-10^{19} Pa·s at the depth of 700 km. The result suggests that the subducting slab is much softer than the surrounding lower mantle (10^{21}-10^{23} Pa·s) inferred from post-glacial rebound. The grain size of perovskite in the lower mantle is estimated to be 1-10 mm, which suggest diffusion creep is dominant deformation mechanism in the large part of lower mantle.

Contents

1. Introduction

Dynamics of the earth's interior depends on the rheological properties of its constituent materials. Pressure-induced phase transition from spinel, $(Mg,Fe)_2SiO_4$, to perovskite, $(Mg,Fe)SiO_3$, plus magnesiowüstite, (Mg,Fe)O, separates the upper and lower mantle relevant to the 670 km seismic discontinuity (Dziewonski and Anderson, 1981; Kennett and Engdahl, 1991) (fig. 1-1). The lower mantle is most likely composed of primarily $(Mg,Fe)SiO_3$ perovskite with certain amounts of (Mg,Fe)O magnesiowüstite (and $CaSiO_3$ perovskite) (*e.g.*, Ringwood and Major, 1971; Knittle and Jeanloz, 1987; Mao *et al.*, 1989, Ringwood, 1991) (fig. 1-2). These three components probably account for 95% of volume of the mantle (Anderson, 1989). The comparison with pressure-volume-temperature equations of state and thermoelastic properties of lower mantle minerals and the seismically observed density and bulk sound velocity profiles of the lower mantle indicate that perovskite may exceed 85 % of its volume (Stixrude *et al.*, 1992). Thus the rheological properties of the lower mantle, which control the dynamics, is determined largely by those of perovskite. However, the rheological properties of the lower mantle depend on that of magnesiowüstite if it occurs as interstitials between perovskite grains because magnesiowüstite may significantly reduce the strength of the lower mantle (Karato, 1981; Handy, 1994).

Plastic deformation of rocks occurs either by motion of dislocations (dislocation creep) or by the diffusive transport of individual atoms (diffusion creep) (Poirier, 1985). Deformation by dislocation creep causes a significant amount of lattice preferred orientation because particular slip systems control the deformation, but diffusion creep

does not (Karato *et al.*, 1995a; Karato, 1988). The measured elastic anisotropy of perovskite (Bass, 1984; Yeganeh-Haeri *et al.*, 1989, 1994) suggested that the preferred orientation of perovskite can produce a detectable seismic anisotropy in the lower mantle (for example, Yaganeh-Haeri (1994) reported that $A_p(=(V_{pmax}-V_{pmin})/V_{pave})$ = 0.07 and $A_s(=(V_{smax}-V_{smin})/V_{save})$ = 0.18 where V_{pmax} and V_{smax} are maximum of measured P- and S-wave velocities respectively, V_{pmin} and V_{smin} are minimum of measured P- and S-wave velocities respectively and V_{pave} and V_{save} are the average of measured P- and S-wave velocities respectively). Based on the shear wave splitting, Meade *et al.* (1995) concluded that the magnitude of anisotropy in the lower mantle was less than 1/100 of that of the upper mantle and the lower mantle was effectively isotropic. The measured elastic anisotropy of olivine, which mainly constitutes the upper mantle, is about five times as large as that of perovskite (Kumazawa and Anderson, 1969). It can be considered that there is little preferred orientation of minerals in the lower mantle. Therefore, the lack of the seismic anisotropy of the lower mantle may give a supporting evidence for prevalence of the diffusion creep mechanism in the lower mantle. Karato and Li (1992) and Li *et al.* (1996) conducted the deformation experiment of $CaTiO_3$ perovskite as an analogue material of $MgSiO_3$ perovskite, and suggested that the dominant deformation mechanism in perovskite may be the lattice diffusion creep (Nabarro-Herring creep) at lower mantle conditions when the average grain size is less than the millimeter order. Karato *et al.* (1995a) reported that a fine-grained sample (8 μm) was deformed by the diffusion creep at conditions of pressure of 300 MPa, temperature of 1498 K and shear strain rate of 4×10^{-5} sec^{-1} and shear strain of 173 %, on

the other hand, a coarse-grained sample (70 μm) was deformed by the dislocation creep at conditions of pressure of 300 MPa, temperature of 1498 K and shear strain rate of 18×10^{-5} sec^{-1} and shear strain of 310 %. Although the experimental strain rate of $\sim10^{-5}$ sec^{-1} is much larger than that in the mantle, these results also suggest that the dominant deformation mechanism is diffusion creep when grain size is small.

In the diffusion creep regime, the effective viscosity is independent of the applied stress and therefore the flow can be regarded as the Newtonian viscous fluid (Karato and Li, 1992; Raj and Ashby, 1971). The effective viscosity can be described as a function of diffusivity of species involving the material, temperature and the grain size (Raj and Ashby, 1971). On the other hand, in the dislocation creep regime, the viscosity is independent of the grain size but it depends on the applied stress together with temperature and .

Recently, some seismic tomographic studies reveal that high-velocity anomalies may correspond to a cold and subducting slab penetrating or sinking into the lower mantle (Silver and Chan, 1986; Fischer et al, 1988; Fukao *et al.*, 1992; Van der Hilst *et al.*, 1991, 1997). As well as the phase transformation from olivine to spinel (Rubie, 1984), a significant grain size reduction should occur in the subducted slab because of phase transformation from spinel to perovskite and magnesiowüstite (Ito and Sato, 1991) when a subducting slab passes through the 670 km discontinuity. The grains of perovskite and magnesiowüstite start to grow after this transformation. Because rheological properties strongly depend on grain size, grain growth rates of perovskite plus magnesiowüstite are important factors for understanding the rheology of the lower

mantle (Karato, 1986; Karato and Li, 1992).

Most of previous works about rheological properties on perovskite analogues have been focused on single crystals (Poirier *et al.*, 1983; Beauchesne and Poirier, 1989; Poirier *et al.*, 1989; Wright *et al.*, 1992; Wang *et al.*, 1993). In contrast, some of works on polycrystals of perovskite analogues was investigated (Karato and Li, 1992; Karato *et al.*, 1995a; Hoshikuma *et al.*, 1995; Li *et al.*, 1996). It is very important to study rheological properties in polycystalline aggregates because the viscosity depends on the grain size in the diffusion creep regime. $MgSiO_3$ perovskite is stable only at high pressures (Ito and Takahashi, 1987) and the direct determinations of rheological properties of $MgSiO_3$ perovskite under its stable conditions are difficult. Thus, rheological properties of perovskite under lower mantle conditions have been deduced based on the results of experiments using analogue materials. However the diffusion creep rate is sensitive to the individual species which compose the materials, and thus the direct experimental determination of the lower mantle materials is very needed.

In the present study, two series of high pressure and temperature experiments was conducted to determine directly the rheological properties of $MgSiO_3$ perovskite in the lower mantle conditions. One is the grain growth experiments, the other is diffusion experiments. In a series of grain growth experiments, forsterite and enstatite was used as the starting material for the grain growth of single phase and two phase aggregates, respectively. In a series of diffusion experiments, silicon self-diffusion in perovskite was conducted. It has been considered that the diffusion of silicon is a controlling mechanism of the diffusion creep of perovskite, because the diffusion of silicon is much

slower than those of other ions in silicate crystals in most of the silicates (Muehlenbachs and Kushiro, 1975; Jaoul *et al.*, 1981, 1983; Houlier *et al.*, 1988; Fisler *et al.*, 1997). Further, the fact that an activation energy for the diffusion creep of $CaTiO_3$ perovskite is equivalent to that for titanium self-diffusion in $CaTiO_3$ perovskite suggests that the self-diffusion of titanium in $CaTiO_3$ perovskite is a rate controlling factor to the diffusion creep of $CaTiO_3$ perovskite (Li *et al.*, 1996). Therefore, the silicon diffusion in $MgSiO_3$ perovskite may be very important for understanding the rheology of the lower mantle.

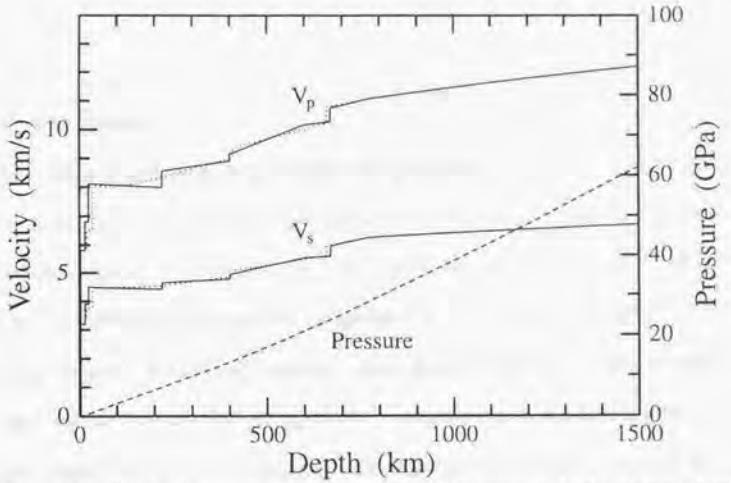

Fig. 1-1. Standard seismic velocity profiles, and pressure-depth relation. Solid lines and dotted lines show the PREM model (Dziewonski and Anderson, 1981) and iasp91 model (Kennett and Engdahl, 1991), respectively. Dashed line show the pressure increase with depth from PREM. The 670 km discontinuity separates the upper and lower mantle.

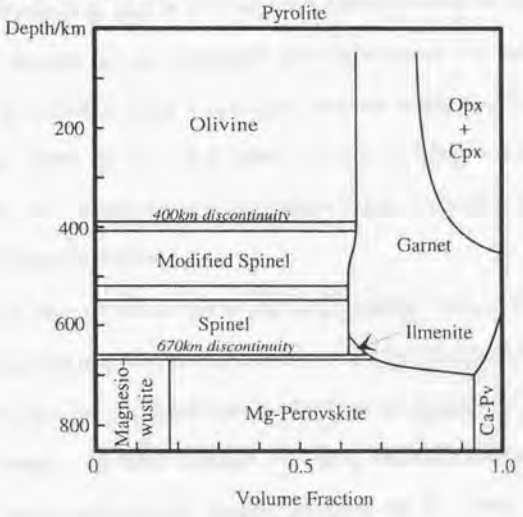

Fig. 1-2. Mineral assemblages of pyrolite composition to a depth of 850 km. It is assumed that the temperature at 400 km is near 1400°C and at 670 km is near 1600°C in accordance with the mantle geotherm. Perovskites and magnesiowüstite constitute the deeper mantle than 670 km. Modified after Ringwood (1991).

2. Experiment

2.1. High pressure and high temperature generation

High pressure experiments were performed using a multianvil apparatus. A large DIA type cubic guide block system driven by a 3000 ton uniaxial press at Tohoku University. The DIA type cubic guide block system was designed and manufactured by TRY Engineering Co., Tokyo, and it enables to drive the multianvil system with 26 mm edge cubes routinely up to 1300 ton (fig. 2-1). The truncated edge length of anvils of DIA type guide block (the first stage) is 50 mm. All experiments were conducted by using the multianvil apparatus with a 2.0 mm anvil truncation (truncated edge length = TEL) which consists of tungsten carbide (WC) (Ohtani *et al.*, 1997) . Twelve pieces of performed pyrophyllite gaskets of 2.0 mm thick and 4.0 mm wide were used (fig. 2-2).

The pressure at high temperature was calibrated on the basis of the phase boundary at 1873 K of ilmenite-perovskite transition in $MgSiO_3$ (Yusa *et al.*, 1993; Kato *et al.*, 1995) and spinel-post spinel transition in Mg_2SiO_4 (Ito and Takahashi, 1987) (fig. 2-3). The uncertainly of the pressure at high temperature is estimated to be about 1 GPa around 25 GPa.

The furnace assemblies used in this study, as shown in Fig. 2-4, are composed of a sintered zirconia pressure medium, a $LaCrO_3$ heater and Mo electrode. A graphite was used as sample capsule, which rapidly transform to diamond in the experimental pressure range (> 20 GPa). Diamond has higher thermal diffusivity than any other ceramics and it may reduce the thermal gradient in the run charge. Temperature was monitored with a W3%Re-W25%Re thermocouple located in the furnace without the

correction of pressure effect on emf of the thermocouples. During runs, temperature was kept within 10°C of a desired value. The measured thermal gradient of the sample at 1873 K is estimated to be less than about 50°C.

2.2. A series of grain growth experiments procedure

Annealing experiments were conducted at pressures up to 25 GPa to determine grain growth rates of aggregates of perovskite ($MgSiO_3$) and periclase (MgO), using a multianvil apparatus. The starting material was synthesized of pure forsterite by heating the stoichiometric mixtures of reagents (MgO : Junsei Chemical Co. Ltd., SiO_2 : Wako Pure Chemical Industries Ltd.) for 45 hours at 1600°C in air. Another starting material, which is enstatite, was synthesized from the stoichiometric oxide mixtures at pressure of 1.5 GPa and temperature of 1550°C for 18 hours by using the piston cylinder apparatus. Components of the furnace assembly, expect for graphite capsule and Mo electrode, were dried at 800°C for over several hours before conducting experiments to make the furnace assembly free from water.

A fine powder (>1 μm grain size) of synthetic forsterite aggregates or sintered enstatite surrounded by NaCl were loaded in the apparatus at room temperature and the pressure was increased to 25 GPa, which corresponds to about 700 km depth in the mantle (Dziewonski and Anderson, 1981). Then the sample was heated to the run temperature ranging from 1573 to 2173 K. Run durations at the constant temperature ranged from a few seconds to 1897 minutes. The run with heating duration of a few

seconds was terminated when the temperature reached the prescribed value by shutting off the heating power supply.

The run products were investigated to measure grain sizes with a scanning electron microscope (JEOL JSM-840) at Geological Institute, University of Tokyo using operating condition of accelerating voltage of 20 kV and the beam current of 10^{-9}-10^{-10} A. Chemical analysis of run products were made with an electron microprobe (JEOL JXA-8900) at Geological Institute, University of Tokyo. Typical operating conditions were accelerating voltage of 15 kV and beam current of 1.2×10^{-8} A. An x-ray diffractometer (JEOL DX-MAP2), at Mineralogical Institute, University of Tokyo, was used to identify the each phase. The instrumental conditions were as follows: X-ray beam diameter, 30-100 μm; counting time, 10000 sec; X-ray generator, 35 kV and 25 mA with Cu filter. To investigate the microstructure, a transmission electron microscope observations were carried out with a JEOL JEM-2010EX and a JEM-2000FX using an accelerating voltage of 200 kV at Hokkaido University and at Geological Institute, University of Tokyo, respectively. The double-tilt specimen holder was used.

The grain boundaries were traced on back-scattered electron images (BSE) of thin sections, using computerized image-processing. For a series of grain growth experiments using forsterite as starting material, the grain sizes were estimated from the area of each grain, assuming the irregular grain boundary outlines could be approximated by a circle. Schwartz-Saltykovs method (Saltykov, 1958) was used to estimate the three-dimensional average grain size from the estimated grain areas. For a series of grain growth experiments using enstatite as starting material, the grain size

measurements were made on back-scattered electron images (BSE) of thin sections using the intercept method (Mendelson, 1969). Average grain size was (G) estimated from the measured average intercept length (L) by $G=cL$, where c is 1.56, assuming that the grain size distribution was log-normal distribution (Mendelson, 1969).

2.3. A series of diffusion experiments procedure

To determine the coefficient of silicon self-diffusion in perovskite, $MgSiO_3$ perovskites were first synthesized at 25 GPa and 1973K from single crystals of synthetic enstatite as starting material. The recovered sample was polycrystalline perovskite and the grain size of perovskite was ~20 μm. After synthesis of perovskite, the samples were polished with diamond paste (0.25 μm in diameter) and were cleaned up carefully using ultrasonic cleaner with alcohol, and then they were coated with a ^{29}Si-enriched thin film (a few tens namometer thickness) formed by high vacuum thermal evaporation of an $^{29}SiO_2$ enriched powder (95.65 atomic %, Oak Ridge National Laboratory, USA). The coated perovskites of ^{29}Si film were used for diffusion experiments as starting materials. These perovskites were pressurized up to 25 GPa at room temperature and were heated at a constant rate of 500 °C per minute up to the experimental temperatures (1673 K-2073 K). Prescribed temperature was kept constant during the desired time (1-50 hours). For the both diffusion and synthetic experiments under high pressure, the sample was loaded with NaCl pressure medium in order to suppress the generation of the differential stress. After the annealing, the recovered run charges were carefully washed by pure water to expose ^{29}Si film coated surface.

The annealed perovskite were mounted in epoxy disks to analyze the diffusion profile of ^{29}Si using a secondary ion mass spectrometry (SIMS). The profile was obtained by the depth profile analysis by a Cameca IMF-3F at Tokyo Institute of Technology. The primary ion beam was mass filtered $^{16}O^-$ accelerated to 12.5 keV and adjusted for a beam current of about 40 nA. Secondary intensities of the ions ^{25}Mg, ^{26}Mg, ^{28}Si, ^{29}Si and ^{30}Si from the center area (~60 μm in diameter) of sputtered crater (150×150 μm) were detected in order to eliminate crater edge effect. The depth calibration of the craters was carried out with a surface profiler and/or a multibeam interferometer after SIMS measurements (Yurimoto and Sueno, 1984; Yurimoto et al, 1989).

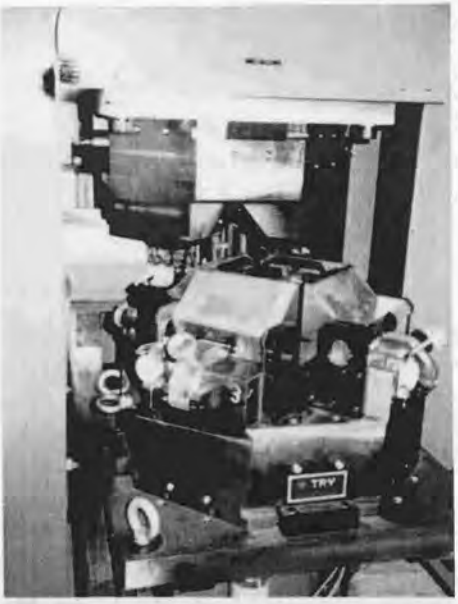

Fig. 2-1. 3000 ton uniaxial press with DIA type guide block system for multianvil apparatus installed at Tohoku University (MAP3000).

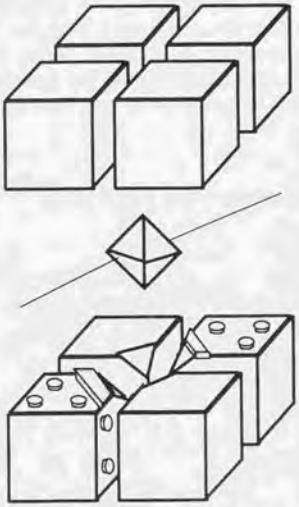

Fig. 2-2. Schematic figure of MA8 system with high pressure apparatus and pressure medium with thermocouple wires. An MA8 is constructed by eight WC anvils with 2 mm truncated edge length (TEL).

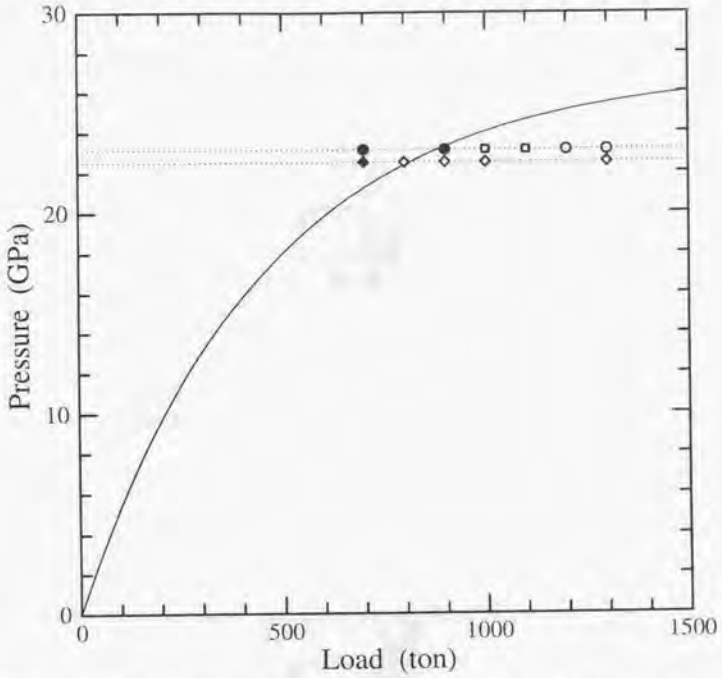

Fig. 2-3. Calibration curve for TEL = 2 mm on the basis of the phase boundary at 1873 K of ilmenite-perovskite transition in $MgSiO_3$ of 22.5 GPa (Kato *et al.*, 1995) and spinel-post spinel transition in Mg_2SiO_4 of 23.1 GPa (Ito and Takahashi, 1987). Open circles, open squares and solid circles represent perovskite + periclase, spinel + perovskite + periclase, and spinel in Mg_2SiO_4, respectively. Open diamonds and solid diamond represent perovskite and ilmenite in $MgSiO_3$, respectively. High pressure experiments in the present study were carried out at load of 1300 ton regarded as 25 GPa.

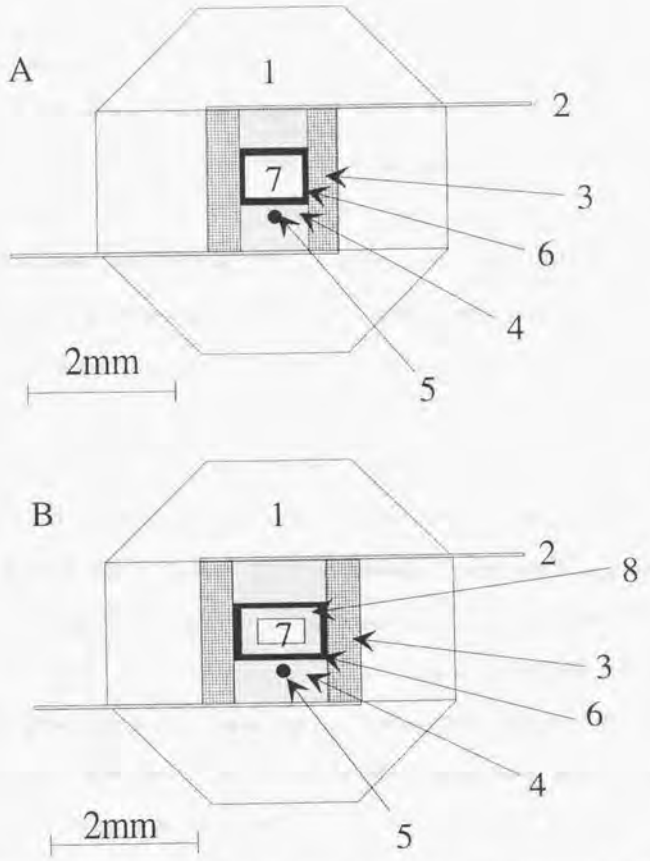

Fig. 2-4. Furnace assemblies for a series of grain growth experiments using forsterite as starting materials (A), and for a series of grain growth experiments using sintered enstatite as starting materials and a series of diffusion experiments (B). 1: ZrO_2 pressure medium; 2: Mo electrode; 3: $LaCrO_3$ heater; 4: (Mg,Co)O insulator; 5: $W_{97}Re_3$-$W_{75}Re_{25}$ thermocouple; 6: graphite capsule; 7: sample; 8: NaCl medium.

3. Results

3.1. Microstructural observation

Annealing experiments were conducted to determine the grain growth rates of aggregates of perovskite ($MgSiO_3$) and periclase (MgO) at pressures up to 25 GPa. temperature ranged from 1573 to 2173 K (heating rate is a constant rate of 100°C per minute) and durations at constant temperatures ranged from a few seconds to 1897 minutes. A fine powder (>1 μm grain size) of synthetic forsterite was used as starting material.

At 25 GPa, the stable phase in Mg_2SiO_4 is spinel structure (low pressure phase) below *ca.* 950 °C but perovskite + rock salt structure (high pressure phase) is stable phase above *ca.* 950 °C, because the phase boundary between Mg_2SiO_4 spinel and $MgSiO_3$ perovskite + MgO periclase has the negative slope (dP/dT) (P (GPa) = 27.6 - 0.0028T (°C)) (Ito and Takahashi, 1989) (fig. 3-1). Therefore, forsterite which was starting material transformed to spinel and then to perovskite + periclase during heating up to desired temperatures. Such phase change was observed in the previous studies (Wang *et al.*, 1997; Martinez *et al.*, 1997).

At low temperature (1573 K) for a few seconds duration, only spinel with equigranular grains was formed, and after 6 minutes heating duration aggregates of perovskite and periclase formed eutectoid-type grains with equigranular spinel grains (fig. 3-2A), and further perovskite + periclase aggregates was formed for 60 min duration. The variations of phases and volume fraction of each phases with time resulted from the kinetics of phase transformation from spinel to perovskite + periclase. For

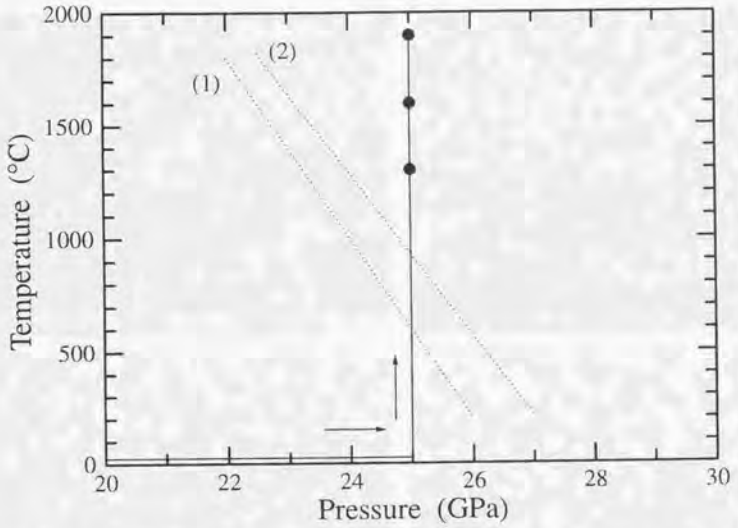

Fig. 3-1. Pressure and temperature path of experiments. Solid circles show the experimental conditions. Dotted lines represent the phase boundaries (1) between ilmenite and perovskite in $MgSiO_3$ to be P (GPa) = 26.5 - 0.0025T (°C) (Kato *et al.*, 1995) and (2) between spinel and post spinel in Mg_2SiO_4 to be P (GPa) = 27.6 - 0.0028T (°C) (Ito and Takahashi, 1987). The P-T paths in experiments undergo the stable fields of lower pressure phases.

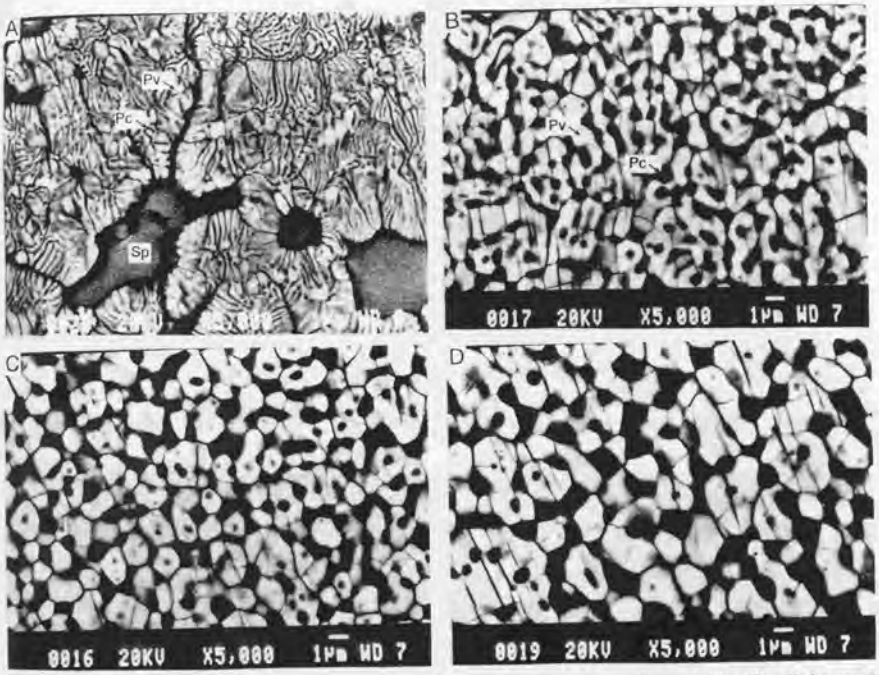

Fig. 3-2. Back scattered electron images of run products. Aggregates of perovskite (Pv, light gray) and periclase (Pc, dark gray) show a homogeneous and equigranular texture, except for (A). (A) Sample from run no. PV20. The coarse grains show γ-spinel with grain size of ~ 10 μm (Sp, gray portion). Perovskite and periclase aggregates show eutectoid texture. (B) Sample from run no. PV17. (C) Sample from run no. PV16. (D) Sample from run no. PV19.

longer-duration (600 min) run, the texture became more uniform and most of grains were equigranular (fig. 3-2B). At high temperature (1873 K ~) for a few seconds duration, perovskite + periclase aggregates were instantaneously formed and the aggregates show equigranular texture (fig. 3-2C), so that high temperature hastens the rate of transformation (*e.g.* Rubie *et al.*, 1990).

A transmission electron microscope observations were carried out with the double-tilt specimen holder to observe the microstructure and to investigate the crytallographic orientation. Unfortunately, it was very difficult to observe $MgSiO_3$ perovskite by a transmission electron microscope, because $MgSiO_3$ perovskite was unstable phase at ambient conditions and it quickly amorphized by the damage of electron beam. In the present study, only several selected-area electron diffraction patterns of perovskite could be obtained (fig. 3-3). Selected-area electron diffraction patterns of perovskite, periclase and spinel were indexed with Pbnm, Fd3m and Fm3m space groups, respectively, showing orthorhombic perovskite.

The run product at 1573 K (run no. PV20) consists of fine intergrowths of perovskite and periclase with host equigranular spinel (Figs. 3-2A, 3-3A). The nucleations of new phases, which were perovskite and periclase, were occurred on the grain boundary between host spinel grains. The electron diffraction patterns revealed no topotaxy between host spinel and periclase nor among periclase grains (fig. 3-4), as well as olivine-modified spinel transformation (Fujino and Irifune, 1992). No topotactic relation in this study was inconsistent with previous study by Wang *et al.* (1997). They reported the following topotactic relations among the three phases: $[100]_{sp}$ // $[100]_{mw}$,

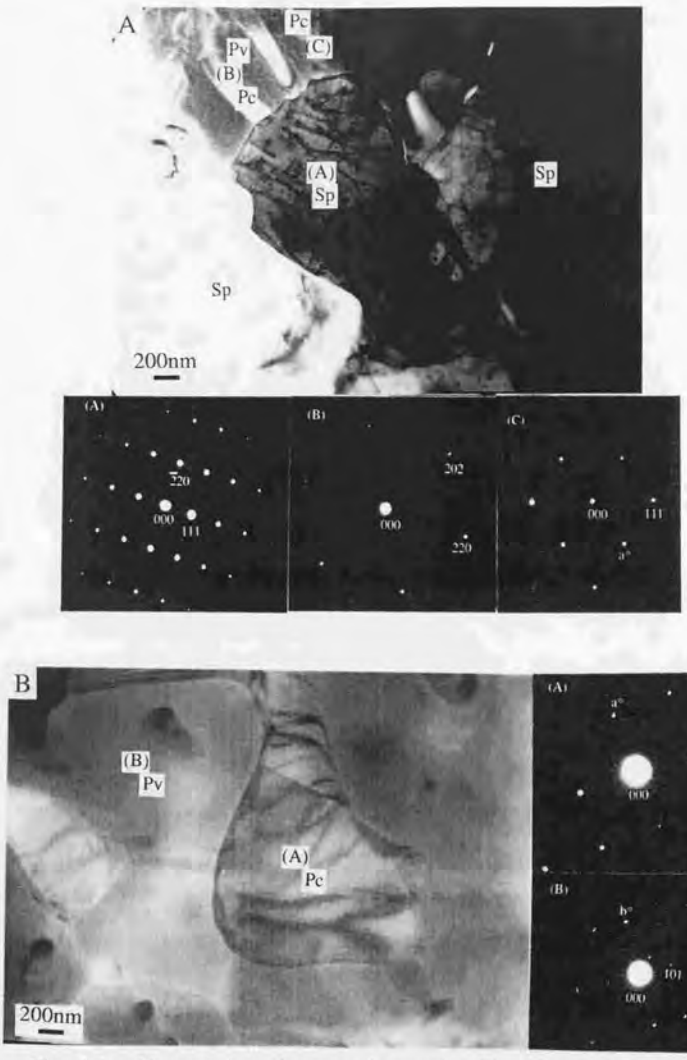

Fig. 3-3. Transmission electron micrographs. The photographs represent partially transformed from spinel to perovskite + periclase (A) (run no. PV20), and completely transformed to perovskite + periclase (B) (run no. PV11), with selected-area electron diffraction patterns of spinel and periclase. The diffraction patterns correspond to the marked grains in the bright field images. Pv: perovskite, Pc: periclase, Sp: spinel.

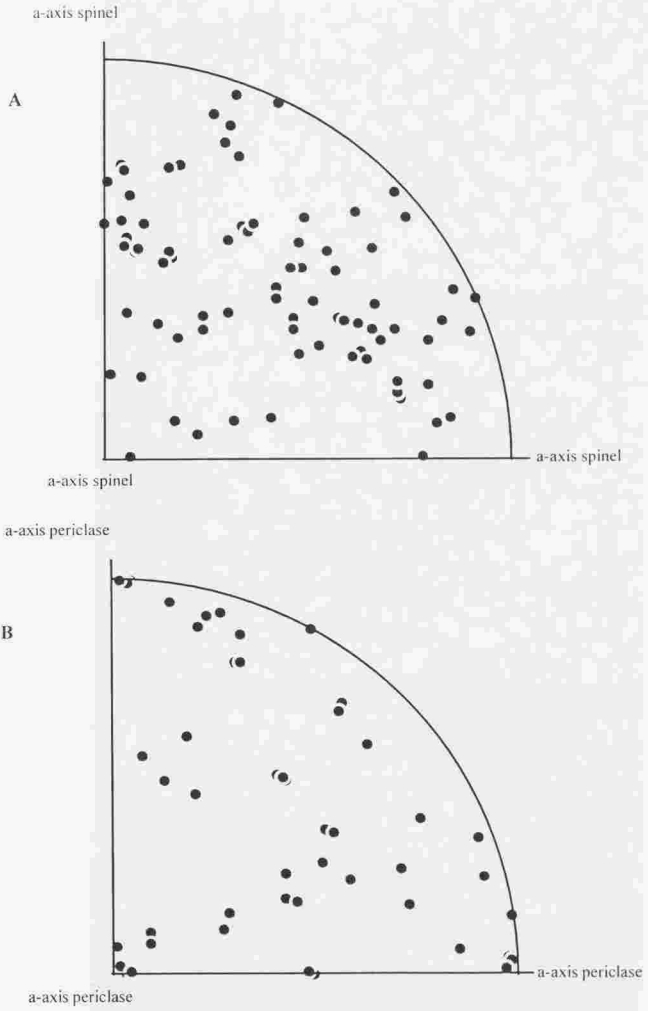

Fig. 3-4. Crystallographic orientations revealed by transmission electron microscope. (A) Showing the relation of lattice orientation between spinel and periclase in equal area projection, (B) showing the relation of lattice orientation between periclases in equal area projection.

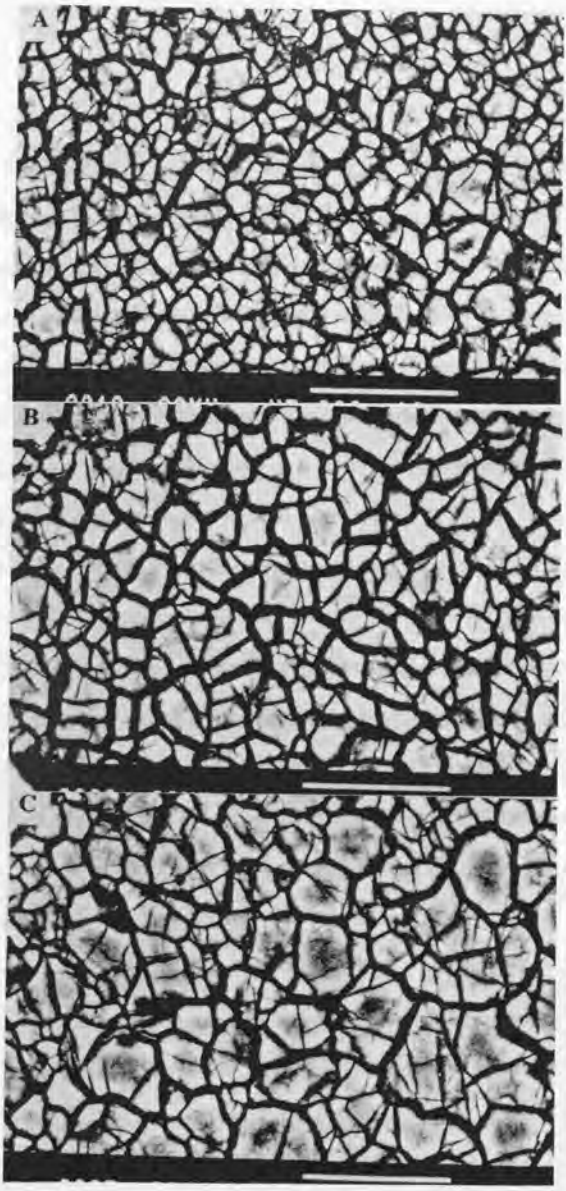

Fig. 3-5. Back scattered electron images of run products. Perovskite (light portion) shows equigranular and homogeneous texture. (A) Sample from run no. PVEN18 at 1873 K for 6 min. (B) Sample from run no. PVEN20 at 1873 K for 60 min. (C) Sample from run no. PVEN23 at 1873 for 600 min. Scale bar: 10 μm.

$[010]_{sp}$ // $[010]_{mw}$, $[001]_{sp}$ // $[001]_{mw}$ and $[100]_{mw}$ // $[1\bar{1}0]_{cpv}$, $[010]_{mw}$ // $[11\bar{1}0]_{cpv}$, $[001]_{mw}$ // $[001]_{cpv}$, where sp, mw, and cpv indicate spinel, magnesiowüstite and cubic perovskite, respectively. The orthorhombic perovskite structure can be derived from the cubic form by continuous tilting of the SiO_6 octahedra, with the general topology remaining unchanged (Wang *et al.*, 1990). TEM examination was conducted using the run product at 1873 K (run no. PV11) with equigranular perovskite and periclase (fig. 3-3B). Although electron diffraction patterns of perovskite are not enough to discuss, it seems to be no topotaxy between perovskite and periclase.

The run products, using enstatite as starting material, consisted of only equigranular grains of perovskite (fig. 3-5). The texture of the polycrystalline perovskite shows more straight grain boundary between perovskite grains (fig. 3-2) rather than that between perovskite and periclase grains in their aggregates (fig. 3-5). It seems that there is no change of the shape of perovskite grains with time. As shown in fig. 3-5, the grain boundary between perovskite grains was characterized by the thick boundary, on the other hand, the thin boundary might represent the crack caused by decompression during the experiment.

3.2. Grain growth of perovskite and periclase in their dual phase

The grain size distributions of perovskite in perovskite + periclase aggregates showed almost log-normal distribution – Lifshitz-Slyozov-Wagner (LSW) distribution (fig. 3-6), suggesting that normal grain growth was occurred and that the driving force was grain boundary energy (Lifshits and Slyozov, 1961; Wagner, 1961). During grain

growth, the patterns of grain size distribution did not much change and the grain boundary energy was reduced by the increases of grain size. The standard deviations of grain size distributions, σ, which represent the shape of size distribution, increase with increasing annealing time from 0.15 to 0.5 (fig. 3-7).

The grain sizes of perovskite and periclase increased with increasing duration and temperature (fig. 3-2, Table 3-1). The grain size of periclase of run no. PV10 (at 1573 K for 10 hours) was not determined because their grain size was less than 0.5 μm and could not be measured. The rate equation was applied for normal grain growth (Burke, 1949; Brook, 1976; Hillert,1965; Glaeser,1984).

$$G^n - G_0^n = G^n\left\{1-\left(\frac{G_0}{G}\right)^n\right\} = kt \qquad (3.1)$$

where G_0 is the initial average grain size, n (>2) is the grain growth exponent, and k is the growth rate constant having a Arrhenius type dependence on temperature,

$$k = k_0\exp(-Q/RT) \qquad (3.2)$$

where k_0 is the pre-exponential factor and Q is the activation energy of grain growth. For $G_0 < G$, the law may be written as

$$G^n = kt \qquad (3.3)$$

therefore, the equation (3.1) is rewritten as,

$$G^n = k_0t\exp(-Q/RT) \qquad (3.4)$$

At 25 GPa, γ-spinel was formed at temperatures less than 1573 K. The grain size of γ-spinel was several micrometers. The γ-spinel partially transformed (about 80% by volume) into perovskite (about 55% by volume) plus periclase (about 25% by volume)

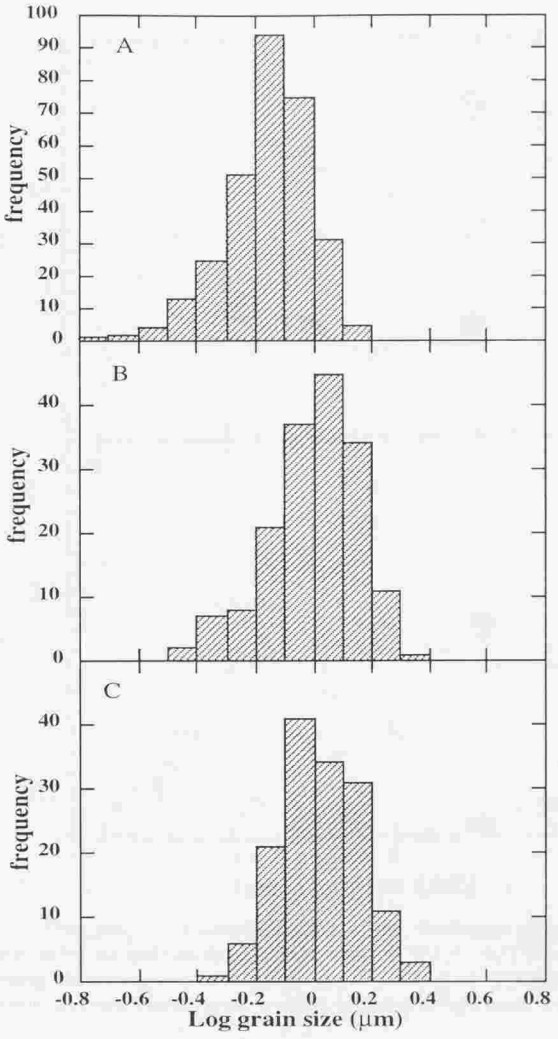

Fig. 3-6. Log-normal grain size distributions of perovskite. The samples, which were used forsterite as starting material, annealed at 25 GPa and 1873 K for 0 min (A, run no. PV15), for 60 min (B, run no. PV11) and for 600 min (C, run no. PV18). 302 (A), 167 (B) and 149 (C) grains were measured.

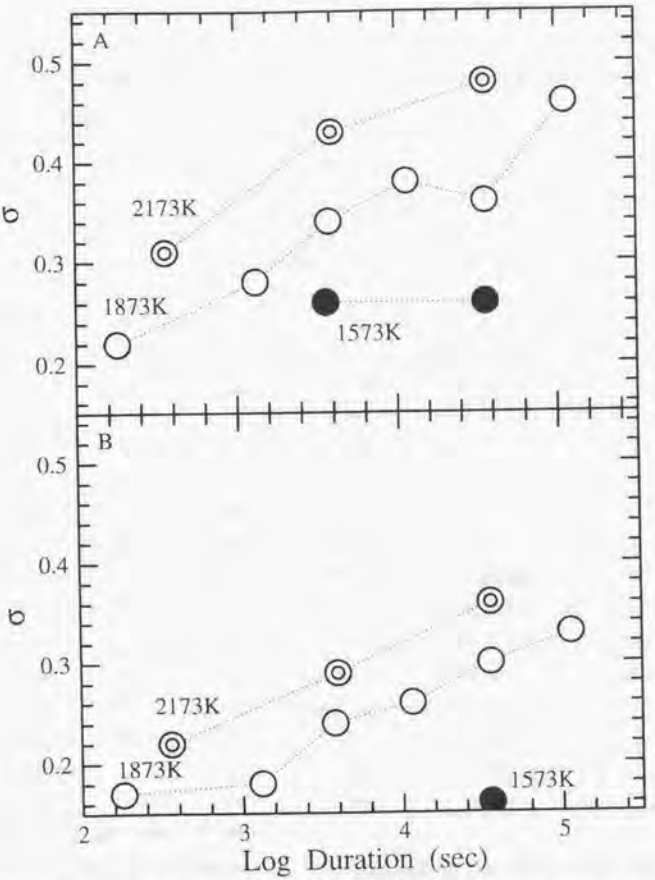

Fig. 3-7. The change of standard deviation of the distribution of grain size, σ (1σ) perovskite (A) and periclase (B) with time at 1573 K, 1873 K and 2173 K, respectively. According to bifurcation theory (Miyazaki *et al.*, 1986), the standard deviation of size distributions must decrease with increasing annealing time.

Table 3-1. Experimental conditions and calculated average grain size for perovskite and periclase. For each experiments was held at 25 GPa at constant temperature (T) for the given duration.

Run no.	T (K)	Duration (min)	Phase*	Grain size, Pv‡ (μm)	Grain size, Pc‡ (μm)
		starting material : forsterite			
PV13	1573	f.s.†	γ	n.d.††	n.d.††
PV20**	1573	6	γ + Pv + Pc	n.d.††	n.d.††
PV10	1573	60	Pv+Pc	0.75 (0.26)	n.d.††
PV17	1573	600	Pv+Pc	0.92 (0.26)	0.67 (0.16)
PV15	1873	f.s.†	Pv+Pc	0.88 (0.22)	0.67 (0.17)
PV22	1873	19	Pv+Pc	1.03 (0.28)	0.80 (0.18)
PV11	1873	60	Pv+Pc	1.29 (0.34)	1.07 (0.24)
PV21	1873	190	Pv+Pc	1.27 (0.38)	1.03 (0.26)
PV18	1873	600	Pv+Pc	1.30 (0.36)	1.07 (0.30)
PV23	1873	1897	Pv+Pc	1.69 (0.46)	1.15 (0.33)
PV16	2173	f.s.†	Pv+Pc	1.10 (0.31)	0.82 (0.22)
PV12	2173	60	Pv+Pc	1.61 (0.43)	1.12 (0.29)
PV19	2173	600	Pv+Pc	1.72 (0.48)	1.29 (0.36)
		starting material : enstatite			
PVEN18	1873	6	Pv	1.48	-
PVEN20	1873	60	Pv	2.88	-
PVEN23	1873	600	Pv	3.52	-

* : γ, Spinel; Pv, perovskite; Pc, periclase

** : Spinel, perovskite and periclase were observed in this run. Grains were not equigranular but formed a eutectoid texture.

† : Run duration is a few seconds.

†† : Not determined because their grain size was less than 0.5 μm and could not be measured.

‡ : Schwartz-Saltykov's method (1958) was used for calculating the three-dimensional average grain size. Numbers in parentheses are the standard deviations for the grain size distributions.

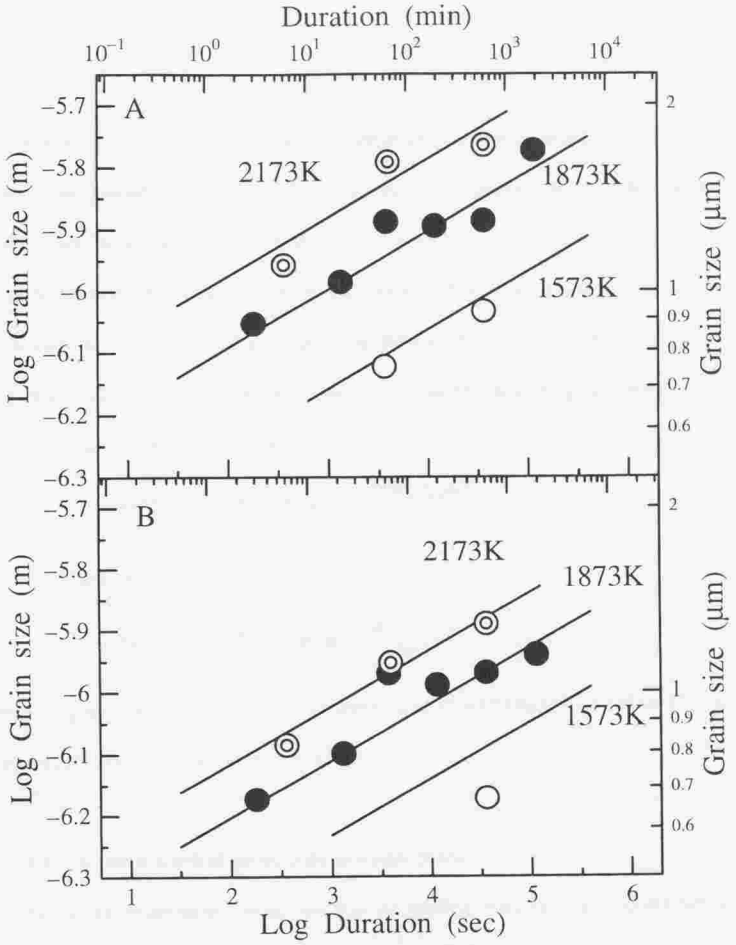

Fig. 3-8. Grain size changes with time. Open circles, solid circles and w-circles show the grain size at 1573 K, 1873K and 2173 K respectively. Solid lines represent the best fit to grain growth law (eqn. 3.4), providing the growth exponents n and the activation energies Q to be 10.6 and 320.8 kJ/mol for perovskite (A), respectively, and 10.8 and 247.0 kJ/mol for periclase (B) respectively.

at 1573 K after 6 minutes. From these observations, it was assumed that the grain growth of perovskite and periclase started at time, t_0=6 minutes, at 1573 K and that perovskite and periclase in contact with γ-spinel was the initial texture (Figs. 3-2A, 3-3A). If the thickness and spacing of these perovskite and periclase grains represents G_0, G_0 is always less than about 0.2 μm, satisfying the condition, $G_0<G$. A least squares fit to the experimental results (Table 3-1) gives n, k_0 and Q. Thus the grain growth rates were estimated for perovskite as (eqn. 3.4),

$$G^{10.6\pm1.0} = 10^{-57.4\pm5.9} t \exp\left(-\frac{320.8 \pm 33.9}{RT}\right) \qquad (3.5)$$

and for periclase as,

$$G^{10.8\pm1.9} = 10^{-62.3\pm11.6} t \exp\left(-\frac{247.0 \pm 55.3}{RT}\right) \qquad (3.6)$$

where G is grain size in meter at time t in second and Q (=320.8±33.9 or 247.0±55.3) is the activation energy of grain growth in kJ/mole (fig. 3-8).

3.3. Grain growth of perovskite in single phase

Annealing experiments using enstatite as starting material were conducted to compare the grain growth rates in single phase of $MgSiO_3$ perovskite with that in dual phase of $MgSiO_3$ perovskite + periclase aggregates at pressures up to 25 GPa, at constant temperature of 1873 K (at a constant rate of 200°C per minute) and durations from 6 minutes to 600 minutes. The phase boundary in $MgSiO_3$ between ilmenite (low pressure phase) and perovskite (high pressure phase) is determined to be P (GPa) = 26.5 - 0.0025T (°C) (Kato *et al.*, 1995) (fig. 3-1). The stable structure in $MgSiO_3$ was

ilmenite type at 25 GPa and below about 600 °C, however it seems that temperature of <600 °C is too low to transform from enstatite to ilmenite. In the present study, perovskite was only observed without ilmenite and enstatite.

The grain sizes of perovskite increased with increasing heating duration (fig. 3-5). In run products, there was no grain which suggested abnormal grain growth. The rate equation for normal grain growth was applied as well as the grain growth of perovskite and periclase aggregates, assuming that the grain size distribution was log-normal distribution.

At 1873 K, the lower limit of the stability field of perovskite in $MgSiO_3$ is lower about 1 GPa than that of perovskite + periclase in Mg_2SiO_4 (Ito and Takahashi, 1989; Kato *et al.*, 1995). At 25 GPa, the rate of transformation from enstatite to perovskite may be much larger than that from forsterite to spinel and to perovskite and periclase because the overpressure of perovskite phase is larger than that of perovskite + periclase phase. It was assumed that enstatite instantaneously transformed into perovskite and that the grain growth of perovskite started at time when temperature reached 1873 K. And assuming the condition of $G_0<G$, a least squares fit to the experimental results gives the rate of grain growth at constant temperature of 1873 K as (eqn. 3.3),

$$G^{5.3} = 10^{-33.3}t \qquad (3.7)$$

where G is grain size in meter at time t in second (fig. 3-9). The grain growth rate of perovskite in the single phase aggregates is much larger than that in the dual phase aggregates of perovskite + periclase.

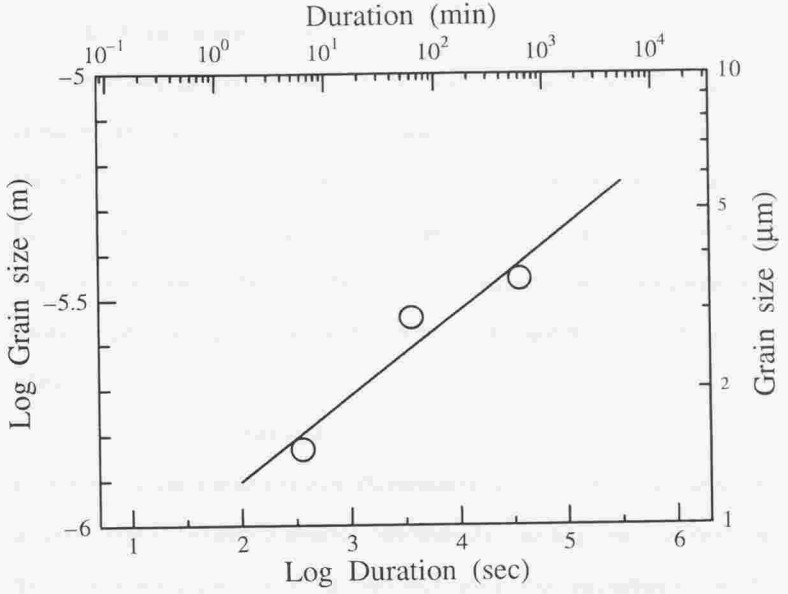

Fig. 3-9. Grain growth of perovskite in its single phase with time. Open circles show the grain size at constant temperature of 1873K. Solid line represents the best fit to grain growth law (eqn. 3.3), providing the growth exponents n to be 5.3.

3.4. Equation of diffusion

Penetration profiles of ^{29}Si from the coated surface of $MgSiO_3$ perovskite aggregates were measured by depth profile method (Yurimoto *et al.*, 1989) (fig. 3-10). The influence of high diffusivity paths, such as grain boundary, has been classified by Harrison (1961) as type A, B and C. Type A diffusion is observed when $(D_l t)^{1/2} \geq G/2$, where D_l is the lattice diffusion coefficient and G is grain size. When this condition is satisfied, a penetration profile can be characterized by a single diffusion coefficient D_A where

$$D_A = (1 - f)D_l + fD_{gb} \tag{3.8}$$

and f is the fraction of grain boundary. D_A represents the coefficient of bulk (effective) diffusion. Type C diffusion is observed only when the annealing time is so short that $(D_l t)^{1/2} << \delta$, where δ is width of the grain boundary. In this case, diffusion from the grain boundary into surrounding body can be neglected and the penetration profile shows a single curve due to grain boundary diffusion. The diffusion is type B and is contributed by both along the grain boundary and in the lattice at following conditions (Atokinson and Taylor, 1979)

$$\delta << (D_l t)^{1/2} \leq G/2 \tag{3.9}$$

In the present study, when the annealing time was short (10 hours) at low temperature (1673 K), the penetration depth was short and the profile was characterized by a single curve, meaning a single diffusion mechanism due to grain boundary diffusion (fig. 3-11A, run no. DIF15). On the other hand, in the case that the annealing time was long or at high temperature, the diffusional profiles displayed the pattern

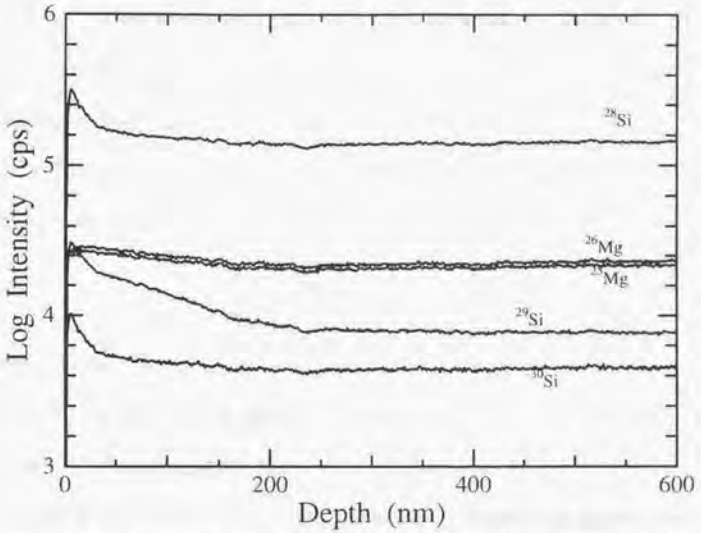

Fig. 3-10. Secondary ion intensities obtained by SIMS measurement of perovskite as a function of penetration after annealing for 10 hours at 25 GPa and 1873 K (run no. DIF14). ^{25}Mg, ^{26}Mg, ^{28}Si, ^{29}Si and ^{30}Si were measured, using ^{29}Si as diffusant species.

composed of two segments (fig. 3-11B): one is the lattice diffusion segment near the surface and the other is the grain boundary diffusion segment at the deeper part. The penetration curve composed of two segments have been often observed in diffusion experiments of polycrystalline matters (Harrison, 1961; Atkinson and Tatlor, 1979).

The lattice diffusion segment was fitted by the following function of diffusion equation with a thin film reservoir of diffusant (Clank, 1975),

$$c - c_0 = \frac{M}{\sqrt{\pi D_l t}} \exp\left(-\frac{y^2}{4 D_l t}\right) \qquad (3.10)$$

where c is the ^{29}Si concentration at depth y, c_0 is the initial ^{29}Si concentration in perovskite, t is the annealing time, D_l is the lattice diffusion coefficient and M is the amount of substance deposited at surface.

The grain boundary diffusion segment in the ^{29}Si profile was analyzed using the following grain boundary diffusion model (Le Claire, 1963),

$$\delta D_{gb} = 0.66 \left\{ \frac{d \ln(c - c_0)}{dy^{6/5}} \right\}^{-5/3} \left(\frac{4 D_l}{t} \right)^{1/2} \qquad (3.11)$$

where δ and D_{gb} are the grain boundary width and the grain boundary diffusion coefficient, respectively. The equation (3.11) is insensitive to the boundary structure (Atkinson and Taylor, 1979). In the present study, the initial grain size of perovskite was about ~20 μm and the final grain size was also ~20 μm without significant grain growth, which was consistent with the grain growth rate of perovskite (eqn. 3.7). Thus the grain growth during annealing hardly affected the penetration profiles.

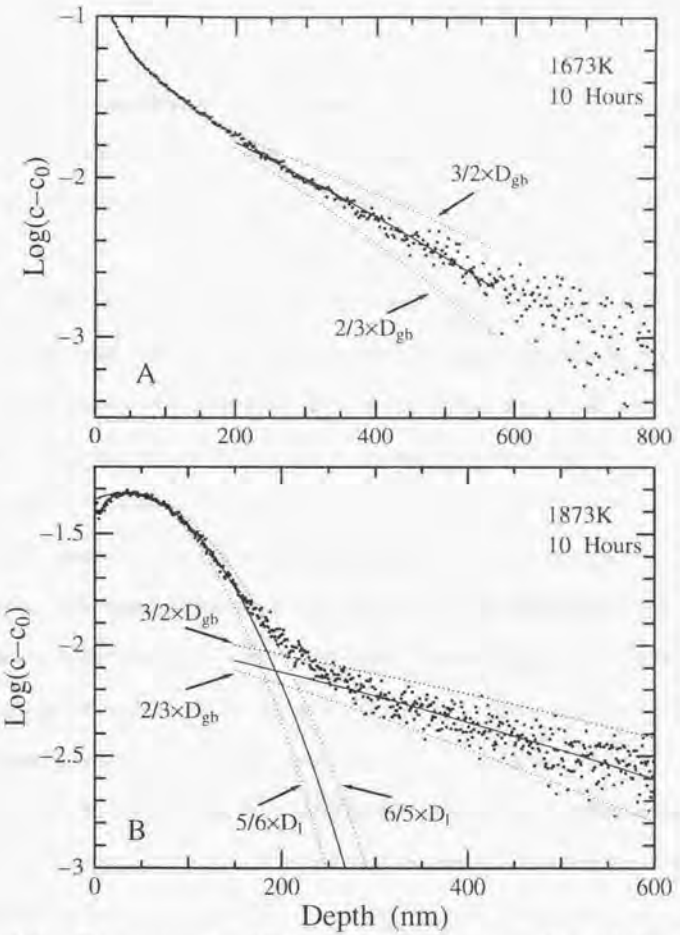

Fig. 3-11. The representative diffusion profiles of ^{29}Si in perovskite including the single segments of grain boundary diffusion contribution, which was annealed at 25 GPa and 1673K for 10 hours (run no. DIF15) (A), and including the two segments, which was annealed at 25 GPa and 1873K for 10 hours (run no. DIF14) (B). (A): The depths between 200 and 570 nm is regarded as the region of the grain boundary diffusion contribution and is fitted to grain boundary diffusion model (eqn. 3.10). Dotted lines represent model profiles using model profiles using 2/3 and $3/2\times D_{gb}$ values of the best fit. (B): It seems that the region from the surface to 30 nm depth is gold thin film layer, and the depths between 30 and 150 nm is the region of the lattice diffusion contribution and between 260 and 600 nm is the region of the grain boundary diffusion contribution. Details in text.

3.5. Si -self diffusion in perovskite

Fig. 3-11B shows the representative diffusion profile of ^{29}Si in perovskite including the two segments, which was annealed at 25 GPa and 1873K for 10 hours. The region from the surface to 30 nm depth is gold thin film layer due to electrostatic charge compensation during SIMS analysis. The depths between 30 and 150 nm is the region of the lattice diffusion contribution and between 260 and 600 nm is the region of the grain boundary diffusion contribution. Solid circles represent the data obtained by SIMS, solid lines represent the best fit to the diffusion model (eqn. 3.10) for the measured profile of the lattice diffusion contribution and the best fit to grain boundary diffusion model (eqn. 3.11) for the measured profile of the region of grain boundary diffusion contribution, respectively. Dotted lines represent the model profiles using 5/6 and $6/5\times D_l$ of the best fit and model profiles using 2/3 and $3/2\times D_{gb}$ values of the best fit, respectively. These model profiles show that D_l and D_{gb} are probably between 5/6 and 6/5 of the best fit value of D_l and between 2/3 and 3/2 of the best fit value of D_{gb}, respectively. The value of $(D_l t)^{1/2}$ estimated for the lattice diffusion coefficient and the annealing time is equal to 6×10^{-8} m, certainly satisfying the condition of Type B (eqn.3.9).

Fig. 3-11A shows the representative diffusion profile of ^{29}Si in perovskite including the single segments of grain boundary diffusion contribution, which was annealed at 25 GPa and 1673K for 10 hours. The depths between 200 and 570 nm is the region of the grain boundary diffusion contribution and deeper part from 570 nm seems to be the background. Solid circles represent the data obtained by SIMS, and solid line

represents the best fit to the grain boundary diffusion model (eqn. 3.10) for the measured profile of the region of grain boundary diffusion contribution. Dotted lines represent model profiles using model profiles using 2/3 and 3/2×D_{gb} values of the best fit.

The sputtered depth calibrated by using a surface profiler and/or a multibeam interferometer may include a uncertainty of less than ±20-30% as shown in fig. 3-12. Fig. 3-13 shows the sample excavated during SIMS analysis. The dark portion was sputtered area by the ion beam.

The diffusion coefficients depend on temperature $D=D_0\exp(-Q/RT)$, where D_0 is the pre-exponential factor in m^2/sec, Q is the activation energy in kJ/mol, R is the gas constant and T is the absolute temperature. The diffusion coefficients were obtained by the least square fit to the experimental results (Table 3-2) as,

$$D_l = 4.12\left(^{+47.7}_{-3.79}\right)\times 10^{-10}\exp\left(-\frac{341\pm 40}{RT}\right) \qquad (3.12)$$

$$\delta D_{gb} = 1.88\left(^{+18.9}_{-1.71}\right)\times 10^{-16}\exp\left(-\frac{310\pm 37}{RT}\right) \qquad (3.13)$$

where, δ is the width of grain boundary (fig. 3-14). As shown in fig. 3-14, uncertainties were smaller than the size of symbols, except for the taking into account an error of depth measurements. An open circle marked by arrow was calculated value (run no. DIF15) because the lattice diffusion coefficient was not determined because the run time was too short. δD_{gb} was calculated by using $D_l=9.28\times10^{-21}$ (m^2/sec) at 1673K and, which was extrapolated from the Arrhenius relationship in fig. 3-14 (eqn. 3.12). There is no remarkable gap in the diffusion coefficients, suggesting no change in diffusion

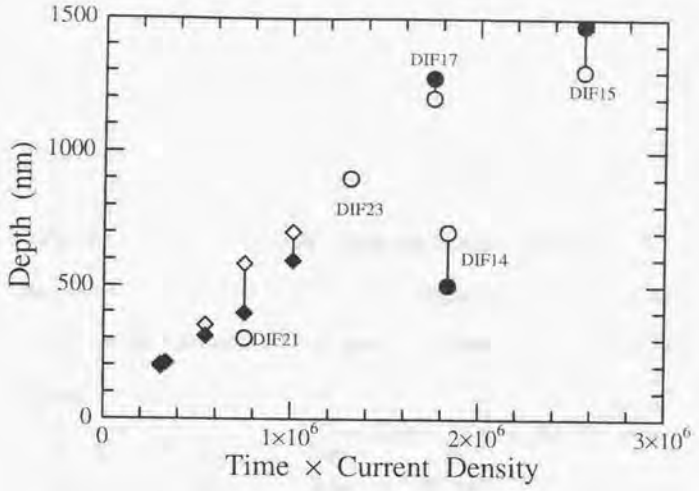

Fig. 3-12. Crater depth formed by sputtering with primary ion current as a function of ion flux per unit area (sputtering time × current density). Circles and diamonds show the depth of perovskite and slide glass, respectively. Open circles and solid circles represent the depths measured with a surface profiler (Dektak) and a multibeam interferometer, respectively. The uncertainties of depth calibration are considered to be ~ 30 %, assuming that the difference between measured depths with a surface profiler and with a multibeam interferometer represents the error of depth calibrations.

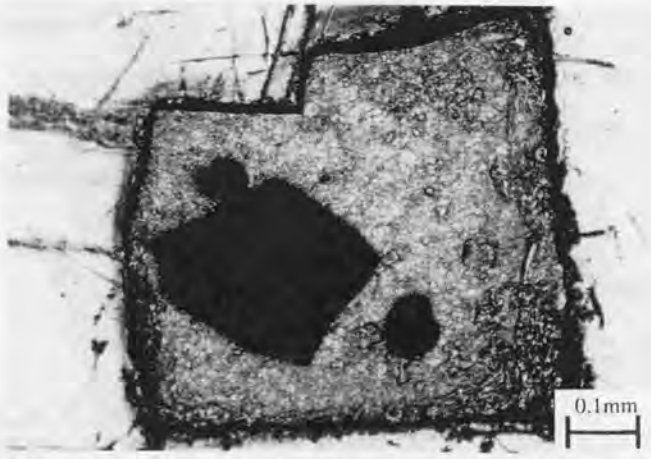

Fig. 3-13. Optical micrograph of $MgSiO_3$ perovskite after SIMS analysis. The dark portion is crater formed by ion beam during SIMS measurement. The crater size is about 150×150 μm.

Table 3-2. Experimental conditions and the diffusion coefficients. All experiments were conducted at 25 GPa at constant temperature for given duration using. The initial and final grain size of perovskite were about 5-20 μm.

Run no.	Temperature K	Time hour	D_l^* m^2/sec	δD_{gb}^{**} m^3/sec
DIF15†	1673	10	-	3.61×10^{-26}
DIF23	1773	50	5.45×10^{-20}	1.94×10^{-25}
DIF14	1873	10	1.01×10^{-19}	3.94×10^{-25}
DIF17	1973	6	4.41×10^{-19}	7.08×10^{-25}
DIF21	2073	1	1.29×10^{-18}	4.11×10^{-24}

* : Lattice diffusion coefficient.

** : D_{gb} is grain boundary diffusion coefficient and δ is the width of grain boundary.

† : D_l was not determined because the run was short duration. D_{gb} was calculated from assumed D_l at 1673K, which was extrapolated from the Arrhenius relationship.

mechanism between intrinsic and extrinsic diffusion over a temperature range from 1673 K to 2073 K.

Considering that the width of grain boundary is approximated by the unit cell size to be 10^{-10}~10^{-9}m (Atkinson and Taylor, 1979), the grain boundary diffusion is about 4–5 orders of magnitude faster than the lattice diffusion. The high diffusivity along the grain boundary or dislocation pipes, rather than in the lattice, is consistent with other metals, oxides and silicate crystal (*e.g.* Turnbull and Hoffman, 1954; Atkinson and Taylor, 1979; Yurimoto *et al.*, 1992; Sakaguchi and Haneda, 1996).

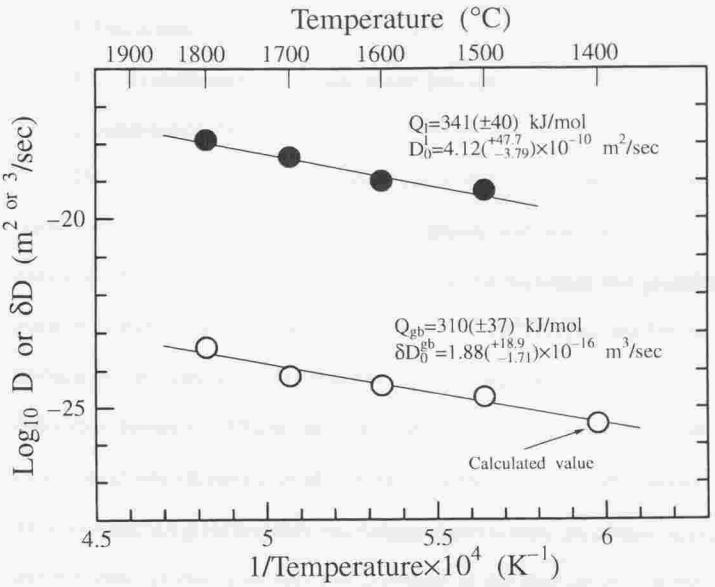

Fig. 3-14. Silicon self-diffusion coefficients in $MgSiO_3$ perovskite plotted against inverse temperature. Solid and open circles represent the lattice diffusion coefficients (D_l) and the products of the grain boundary diffusion coefficient (δD_{gb}) and the width of grain boundary, respectively. Uncertainties were smaller than the size of symbols. Solid lines represent the least square fits to the data. An open circle marked by arrow is calculated value (run no. DIF15).

4. Discussion

4.1. Transformation mechanism and kinetics

Transformation mechanism

The mechanism of transformation from olivine to modified spinel have been considered to be no coherent nucleation and growth with low dislocation density in olivine (~10^7/cm^2), whereas the initiation of coherent nucleation and growth of new phase with high dislocation density in olivine (~10^{10}/cm^2) (Fujino and Irifune, 1992). Dislocation densities is good indicator of the magnitude of differential stress, dislocation density of ~10^7/cm^2 and ~10^{10}/cm^2 at differential stress of 30 MPa and 1 GPa, respectively (Kohlstedt *et al.*, 1976). Kerschhofer *et al.* (1996) suggested that intracrystalline and grain boundary transformation mechanisms are competing processes and that intracrystalline transformation dominates in the large crystals. In the present study, grains of perovskite and periclase start to grow on the grain boundaries between spinel grains during transformation from Mg_2SiO_4 spinel to $MgSiO_3$ perovskite and MgO periclase, and there is no topotactic relations, suggesting that incoherent grain boundary transformation is dominant mechanism rather than coherent (martensitic) mechanism (fig. 3-4). The differential stress should be low because spinel was formed by the transformation from olivine in situ. Small grain size of spinel (~10 μm) and considerable low differential stress suggest the incoherent grain boundary transformation.

The textural evolution during grain growth of perovskite and periclase aggregates with time is consistent with previous observations of the high pressure transition of γ-

spinel to perovskite and periclase (Poirier *et al.*, 1986), suggesting that the transformation starts as a eutectoid texture and becomes more equigranular during grain growth. Ito and Sato (1991) reported that spinel ($(Mg_{0.9}, Fe_{0.1})_2SiO_4$) transformed to perovskite + magnesiowüstite with a eutectoid texture at 24 GPa and 1873 K for 1 hour. The eutectoid texture may be due to the growth of nuclei of new phases, controlled by atomic diffusion toward the interface between the host grain and the new grains which is high-pressure phases (Fournelle and Clark, 1972; Puls and Kirkaldy, 1972). The atomic diffusion toward the reaction interface has high mobility or high driving force rather than the diffusion among host grains and among new grains (Hornbogen, 1972).

Transformation kinetics

The transformation mechanism affects on the kinetics of transformation. The general rate equation derived by Cahn (1956) for transformation by grain boundary nucleation is

$$f = 1 - \exp\left\{-\frac{6.7}{d}\int_0^y \left[1-\exp(-z)\right]dy\right\} \qquad (4.1)$$

where

$$z = -\pi\int_0^{t-t'} N\left\{x^2(t-\tau)^2 - y^2\right\}dt \qquad (4.2)$$

and f is the volume fraction transformed, d is the grain size of host phase, t' (=y/x) is the time for a nucleus to grow to radius y, y' (=xt) is the growth distance after time t, and τ is the time at which a nucleus forms. Here, it is assumed as following; (1) fig. 3-2A shows the texture when the nucleation of perovskite and periclase on the grain boundary

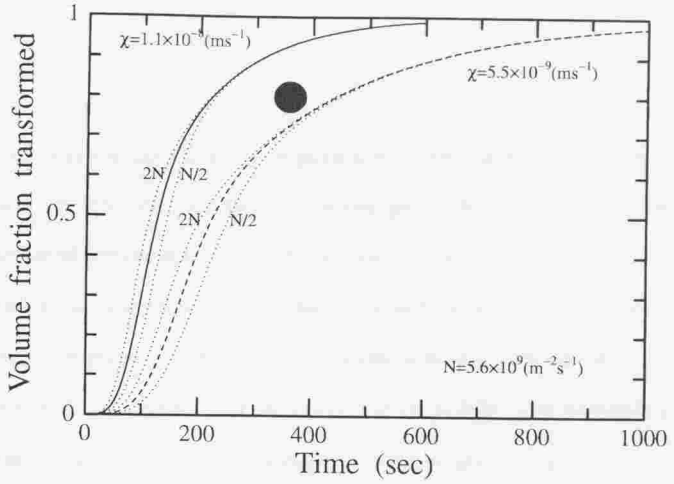

Fig. 4-1. Estimated transformation-time curve (eqn. 4.1). Solid circle represents the data of run no. PV20. Solid line and dashed line show the kinetics with growth rate (x) of 1.1×10^{-8} m/sec and nucleation rate (N) of 5.6×10^{9} /m^{2}sec and growth rate of 5.5×10^{-9} m/sec and nucleation rate of 5.6×10^{9} /m^{2}sec, respectively. Dotted lines represent the cases of $N\times2$ and $N/2$ respectively.

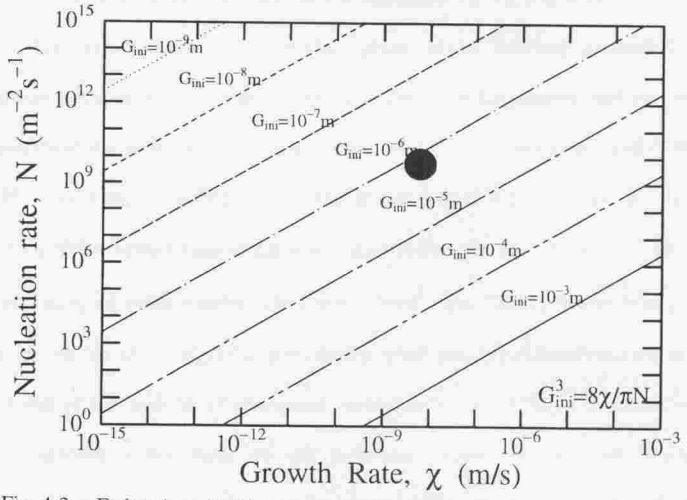

Fig. 4-2. Estimation of initial grain size from the nucleation rate and growth rate. The lines show the each initial grain size of new phase. Solid circle represents the initial grain size at 1573 K calculated from estimated nucleation rate and growth rate in this study.

have just finished, (2) the width of perovskite + periclase phases from the spinel interface, that is length of lamellae, represent the growth distance for $t = 6$ minutes, (3) the number of lamellae was produced by constant nucleation at grain boundary for $t = 6$ minutes. These assumptions lead to obtain the growth rate of 0.5×10^{-8}-1.1×10^{-8} m/sec, assuming that growth rate is constant and homogenous, the grain size of spinel (host grain) is 5-10 μm, and transformed volume fraction is 80%. And nucleation rate is estimated to be 5.6×10^{9} /m^2sec, assuming that thickness and spacing of perovskite and periclase lamellae is 0.2 μm. Fig. 4-1 shows the comparison with calculated transformed fraction applying above assumptions to eqn. (4.1) and experimental result (run no. PV20). Therefore, transformation from spinel with grain size of several micrometers to perovskite + periclase have finished until 15 minutes at 1573 K (fig. 4-1).

The growth rate of the product phase in an interface controlled phase transformation have the Arrhenius type dependence on temperature and the pressure dependence of growth rate given by activation volume is assumed to be small (Turnbull, 1956; Carson and Rosenfeld, 1981). The growth rate of the new phase produced by Ni_2SiO_4 olivine-spinel transformation was determined to be 1.8×10^{-3} m/sec at 1573K by extrapolating of Rubie's result which was $6.5\times10^{11}\exp(-438/RT)$ (Rubie *et al.*, 1990). The growth rate of the Mg_2SiO_4 spinel during spinel-post spinel transformation is lower than that of the Ni_2SiO_4 olivine-spinel transformation at 1573K. The transformation rates obtained in this study are still preliminary results because they depend on conditions of the grain boundary and the applied deferential stress (Rubie *et al.*, 1990), hence more experiments in detail are needed obviously. The initial grain size of new

phase (G_{ini}) is represented as the formula, $G_{ini} = (8x/\pi N)^{1/3}$, where the shape of grain is assumed to be sphere. The initial grain size calculated from the nucleation rate and growth rate is about a order magnitude larger than observed thickness and spacing of lamellae of perovskite and periclase (fig. 4-2), since the nucleation rate may be estimated to be lower than exact value because the nucleation may have already finished at time t = 6 minutes. It is impossible to estimate the initial grain size as function of temperature because of no data of activation energy for growth rate during transformation.

4.2. Grain growth

The grain growth rates were determined to be eqns. (3.5) for perovskite and (3.6) for periclase in two phases aggregates of perovskite + periclase aggregates, and (3.7) for perovskite in the single phase aggregates.

The exponents n = 10.6 and 10.8 for perovskite and periclase, respectively, are larger than those for other silicate minerals and oxides in two phase aggregates; Kapadia and Leipold (1974) reported the grain growth of pure dense MgO, being n = 2 and Q (activation energy) = 277 kJ/mol; Wong (1980) reported the grain growth of ZnO, being n =6 and Q = 243 kJ/mol; Karato (1989) obtained grain growth laws of olivine, being n = 2 or 3 and Q = 160 kJ/mol under wet condition at 300 MPa and n = 2 or 3 and Q = 520-600 kJ/mol under dry condition at 0.1 MPa; Senda and Bradt (1990) reported grain growth of ZnO-4.0 wt% Bi_2O_3, showing n = 5 and Q = 156 kJ/mol; Hoshikuma *et al.*

(1995) reported grain growth law of $MnTiO_3$ and MnO as an analog material of $(Mg,Fe)SiO_3$-perovskite, being $n = 3.55$ and $Q = 560$ kJ/mol.

The geometric factors influence the grain growth exponents. The large exponents indicate how difficult grain growth is and the slow growth rate may be attributed to the spatial distributions of two phases within the aggregates. Here, the presence of two interlocking phases may decrease the grain growth rate of perovskite and periclase due to grain boundary pinning (Nicholson, 1966; Harkulich *et al.*, 1966; Gupta, 1971; Baldo and Bradt, 1988; Chen and Xue, 1990).

The large grain growth exponents cannot be explained by previous models (Nichols, 1966; Hanitzch and Kalweit, 1968). Nichol's model (Nichols, 1966) suggests that grain growth is controlled by a grain boundary drag effect exerted by pores within which the material is transported by surface diffusion to the pore surface. Here, the pore drag mechanism is unlikely to occur, since porosity was not detected in our SEM observations. Hanitzch and Kalweit's model (Hanitzch and Kalweit, 1968) describes grain growth controlled by atomic diffusion along dislocation pipes. Grain growth through diffusion along dislocations is not applicable in our experiments since a high dislocation density probably does not exist in the starting material, which was hot-pressed at high temperature under low differential stress field (see section 4.1).

On the other hand, it has been reported that the grain growth was suppressed significantly, indicating large exponent. Carpenter (1967) observe that the growth exponent for grain growth in Au-Pt alloys strongly depends on chemical compositions, that is, n = 4.8, 9.3, and 3.2 for 40:60, 60:40 and 80:20 Au-Pt alloys, respectively.

Miyazaki *et al.* (1986) proposed a new theory (bifurcation theory) to interpret the large exponent during grain growth. They introduced not only grain boundary energy but also the elastic strain energy and interaction energy between two phases for driving force. According to this theory, the small grains consume the large grains and each grains become uniform size. Therefore, the average grain size increase with increasing annealing time, and the size distribution becomes sharper with increasing annealing time (Miyazaki and Doi, 1989). As shown in fig. 3-7, the standard deviation of the distributions of grain size, σ (1σ), show the patterns which increase with increasing time. It is not obvious whether bifurcation theory is applicable to explain the large growth exponents of perovskite and periclase in this study or not.

The growth exponents for perovskite in dual phases should depend on the contents of perovskite in two phases. The determined exponent for the grain growth of perovskite and periclase, using forsterite as staring material which transformed into perovskite and periclase with the ratio of Pv:Pc = 68:32 in vol., was estimated to be 10-11 and was larger than that of perovskite in single phase (= 5.3). The exponent for the grain growth of periclase in single phase reported to be n=2 at ambient pressure (Kapadia and Leipold, 1974). The exponents for grain growth may change with the ratio of Pv:Pc as shown in fig. 4-3.

The dependence on temperature for grain growth was represented by an activation energy. The activation energy for grain growth is related to that for atomic diffusion because the grain growth in the present study is controlled by atomic diffusion. The activation energy for self-diffusion of oxygen in periclase is 261 kJ/mol by Oishi and

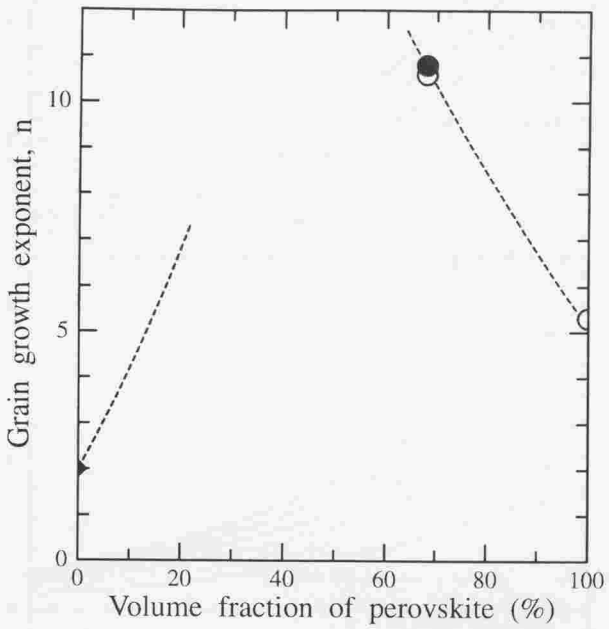

Fig. 4-3. The exponent for grain growth change with the perovskite contents. Open circles and solid circle represent the obtained exponents in this study for growth of perovskite and of periclase, respectively. Solid diamond show the grain growth exponent for periclase by Kapadia and Leipold (1974). Dashed lines show the presumed relation between exponent and perovskite contents.

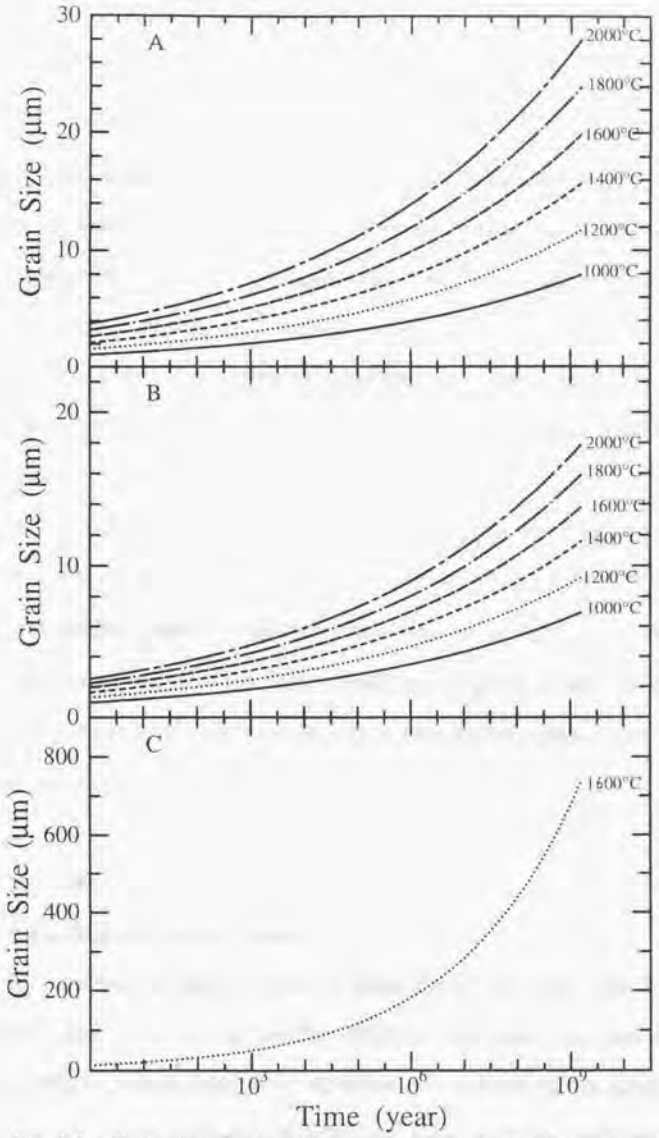

Fig. 4-4. Grain size change with time by extrapolating of experimental results (eqns. 3.5, 3.6 and 3.7) (fig. 3-8, 3-9). (A) Grain growth of perovskite at each temperature (1000-2000°C) in dual phase of perovskite and periclase aggregates, (B) grain growth of periclase at each temperature (1000-2000°C) in dual phase of perovskite and periclase aggregates and (C) grain growth of perovskite at constant temperature of 1600°C in its single phase.

Kingery (1960), 312.6 kJ/mol by Yoo *et al.* (1985) and so on, whereas the activation energy for self-diffusion of magnesium in periclase is 231 kJ/mol by Sakaguchi *et al.*, (1992), 330.7 kJ/mol by Lindner and Parfitt (1957) and so on. Because the activation energy reported for self-diffusion is scattered, the activation energy for grain growth of periclase (247.0 kJ/mol) does not clearly suggest what species governs the grain growth of periclase. The activation energies for grain growth of perovskite and for self-diffusion will be described in a later section.

Fig. 4-4 shows the calculated grain size change with time by extrapolating experimental results as eqn. (3.5), (3.6) and (3.7). The grain size of perovskite in dual phase of perovskite + periclase is less than ~15 μm after grain growth for 1 million years, on the other hand, that in the single phase is more than 100 μm after grain growth for 1 million years. However, the both grain sizes are smaller than the expected grain size in the lower mantle (discussed in section 5).

4.3. Diffusion

Comparison with previous results

The experimental determinations of lattice silicon diffusion coefficients in perovskite (eqns. 3.12, 3.13) are the first reports so that there is no other silicon diffusion data to compare with. Here, the diffusion coefficients are compared with previous results, such as in forsterite, in $CaTiO_3$ perovskite, in enstatite and in periclase (fig. 4-5A). Lattice diffusion coefficient of silicon in perovskite is larger than that in forsterite at ambient condition (Jaoul *et al.*, 1981) and is larger than oxygen in $CaTiO_3$

perovskite at ambient condition (Gaustason and Muehlenbachs, 1993; Sakaguchi and Haneda, 1996). The high diffusivity of silicon in perovskite rather than in forsterite may be understood as resulting from the change of number of Si-coordinate, suggesting that the Si-O bonding of 6-coordinated Si in perovskite may be weaker than that of 4-coordinated Si in forsterite, as well as silicon and oxygen self-diffusion in silicate liquids (Poe *et al.*, 1997).

To compare with diffusion coefficients of magnesium and oxygen in periclase at same pressure, van Liempt's law is used as,

$$Q = BRT_m \qquad (4.1)$$

where T_m is the melting temperature of periclase and B is the constant. The constant of B is calculated to be 5-13 (Lindner and Parfitt, 1957; Oishi and Kingery, 1960; Sakaguchi *et al.*, 1992; Yoo *et al.*, 1985) (Table 4-1) and the self-diffusion coefficients of magnesium and oxygen in periclase at 25 GPa was assumed as shown in fig. 4-5B. The diffusion coefficient of silicon in perovskite is much smaller than that of magnesium in periclase and is similar to that of oxygen in periclase.

The activation energy for lattice diffusion is larger than that for grain boundary diffusion, suggesting that the thermal barrier for jumping of silicon atoms related to the bonding energy in the crystal is higher than that in the grain boundary even at high pressure. The activation energy for grain growth of perovskite (321 kJ/mol) is close to that for lattice diffusion rather than that for grain boundary diffusion, indicating the mass transport along grain boundaries predominantly for grain growth of perovskite in dual phase of perovskite + periclase.

Table 4-1. Diffusion coefficients of oxygen and magnesium in periclase at high pressure estimated by van Liempt's law.

Diffusant	Q_{1atm}* kJ/mol	B**	Q_{25GPa}† kJ/mol	reference
Mg	331	13.0	378	Lindner and Parfitt, 1957
Mg	231	9.1	263	Sakaguchi *et al.*, 1992
Mg‡	139	5.5	159	Sakaguchi *et al.*, 1992
O	261	10.3	298	Oishi and Kingery, 1960
O	313	12.3	357	Yoo *et al.*, 1985

* : Activation energy at 1 atm.

** : The constant in van Liempt's law (eqn. 4.1).

† : Estimated activation energy at 25 GPa, using melting temperature of periclase at 0 GPa and 25 GPa to be 3063 K and 3500 K, respectively (Zerr and Boehler, 1994).

‡ : Grain boundary diffusion.

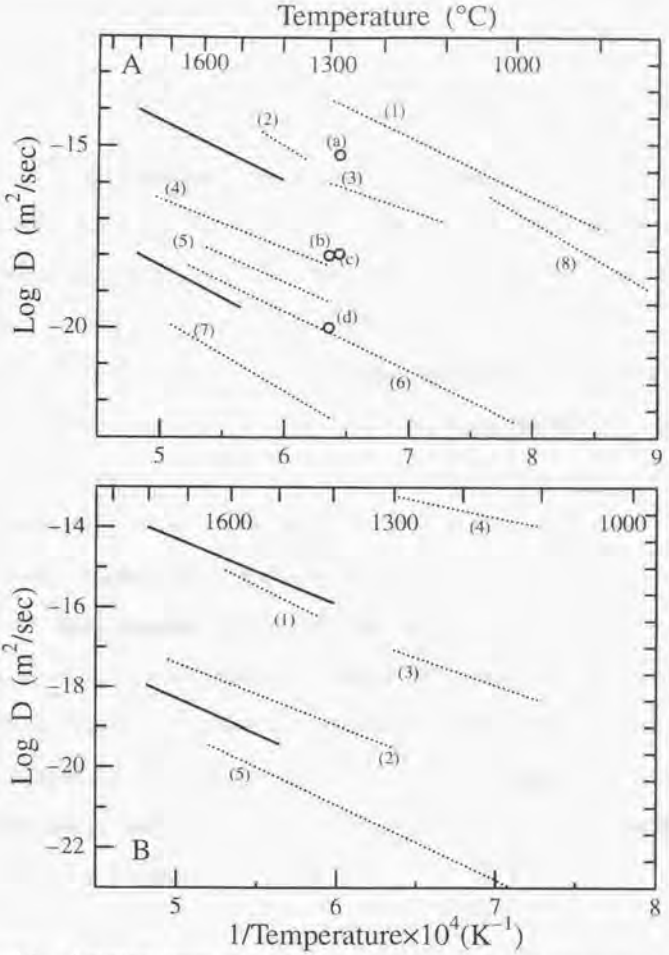

Fig. 4-5. Arrhenius compilation of diffusion coefficients. (A) No corrections were made for difference in pressure. All data show the lattice diffusion coefficients, except for (2), of the experimental data for O in $CaTiO_3$ perovskite (1= Gautason and Muehlenbachs, 1996), effective diffusion of Si in enstatite (2 = Fisher *et al.*, 1997), Mg in periclase (3 = Sakaguchi *et al.*, 1992), O in periclase (4 = Oishi and Kingery, 1960), O in forsterite (5 = Jaoul *et al.*, 1983), O in periclase (6 = Yoo *et al.*, 1985), Si in forsterite (7 = Jaoul *et al.*, 1981), O in $CaTiO_3$ perovskite (8 = Sakaguchi and Haneda, 1996), O in enstatite (a), O in olivine (b), O in forsterite (c), and Si in olivine (d): a and c = Muehlenbachs and Kushiro (1975), b and d = Houlier *et al.* (1988). Solid lines represent the results in this study. (B) Comparison with diffusion coefficients of silicon in perovskite and of oxygen in periclase. Correction for the effect on pressure were made for periclase, using the van Liempt's law (eqn. 4.1, table 4-1). Solid lines represent the coefficients for lattice diffusion and grain boundary diffusion in perovskite, respectively, assuming the width of grain boundary to be 3×10^{-10} m. (1) Mg diffusion (Lindner and Parfitt, 1957), (2) O diffusion (Oishi and Kingery, 1960), (3) Mg diffusion (Sakaguchi *et al.*, 1992), (4) Mg grain boundary diffusion (Sakaguchi *et al.*, 1992), (5) O diffusion (Yoo *et al.*, 1985).

Computer simulation techniques were used to study the defect and diffusion processes in the perovskites $SrTiO_3$, $CaTiO_3$, and $MgSiO_3$ (Wall and Price, 1989; Wright and Price, 1993). Wright and Price (1993) estimated the activation energy for intrinsic diffusion of Schottky type to be 1112.8 kJ/mol in $MgSiO_3$ perovskite. This value is much higher than the value determined here. They described in the paper (Wright and Price, 1993) that the value calculated for intrinsic diffusion is too high to be realistic, and that diffusion may take place by more complex mechanisms than those so far investigated, for example by coupled diffusion or diffusion in the presence of vacancies on another sublattice in real systems.

In general, the lattice diffusion coefficients of same species in different materials have universal law which is the relationship between an activation energies and pre-exponential factors. Fig. 4-6 shows the relationship of universal law of silicon diffusion. The diffusion coefficient of silicon show in perovskite in the present study is plotted on near the line of universal law in the figure, suggesting that the diffusion coefficient in this study is correct value.

Effective diffusion

In polycrystalline materials, the atom transportation is controlled by the effective diffusion (D_{eff}), which represents total mass flux controlled by migration by both in the lattice and along the grain boundary,

$$D_{eff} = D_l + \frac{\pi\delta}{G} D_{gb} \qquad (4.2)$$

where G is the grain size and δ is the width of the grain boundary (Raj and Ashby, 1971). The effective diffusion coefficient is close to the lattice diffusion coefficient when the grain size is large. Whereas, when the grain size is small, the effective diffusion coefficient is close to the grain boundary diffusion coefficient. At high temperatures the effective diffusion coefficient is approximated by the lattice diffusion coefficient. On the other hand, at low temperatures it is close to the grain boundary diffusion coefficient, because the activation energy for the lattice diffusion is smaller than that for the grain boundary diffusion. Estimated effective diffusion coefficients are represented in fig. 4-7, where the width of the grain boundary, δ, is assumed to be 3×10^{-10} m. Above 1000°C, the lattice diffusion is dominant with grain sizes larger than a few micrometers, whereas the effective diffusion is controlled by the diffusion along the grain boundary when the grain size is smaller than a few micrometers.

Furthermore, the effective diffusion in multicomponent materials is controlled by the diffusivities of the each species,

$$D_{\mathrm{eff}} = \frac{1}{\sum_i \frac{\nu_i}{D^i_{\mathrm{eff}}}} \tag{4.3}$$

where ν_i is the stoichiometric coefficients of the i-th compound and D^i_{eff} is the effective diffusion coefficients of i th species (Jaoul, 1990). In the case of $MgSiO_3$ perovskite,

$$\frac{1}{D_{\mathrm{eff}}} = \frac{1}{D_{\mathrm{Mg}}} + \frac{1}{D_{\mathrm{Si}}} + \frac{3}{D_{\mathrm{Ox}}} \tag{4.4}$$

where D_{Mg}, D_{Si} and D_{Ox} are effective self-diffusion of magnesium, silicon and oxygen, respectively. Again, silicon is the slowest diffusion species among other ions in silicate

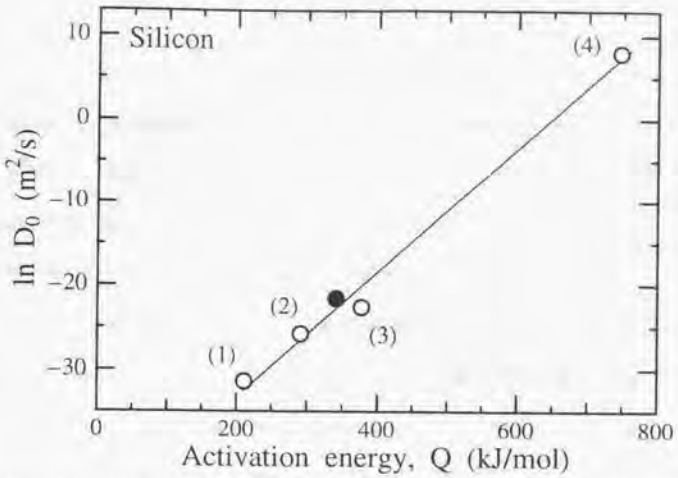

Fig. 4-6. Universal law between activation energies and pre-exponential factors for silicon self-diffusion. Solid circle represents the diffusion in perovskite determined in the present study. (1): in diopside (Béjina and Jaoul., 1996), (2): in San Carlos olivine (Houlier *et al.*, 1990), (3): in forsterite (Jaoul *et al.*, 1981), (4): in quartz (Béjina and Jaoul, 1996).

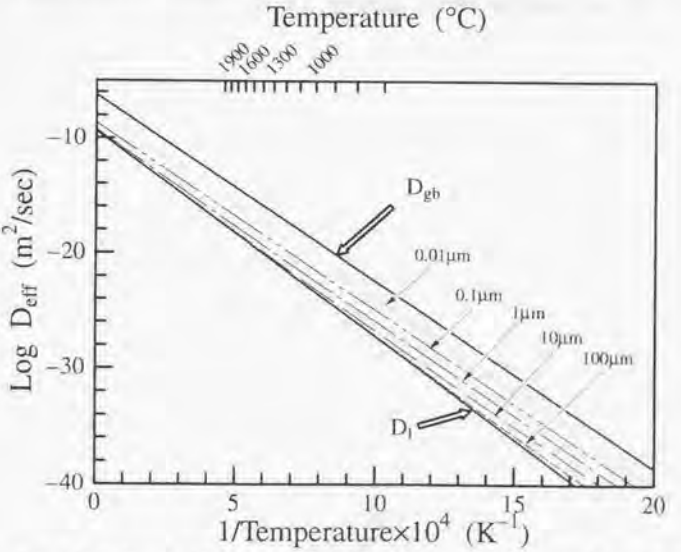

Fig. 4-7. Effective diffusion coefficients as a function of inverse temperature. Thick solid lines show the diffusion coefficients in lattice and along grain boundary, respectively. Thin lines represent the effective diffusion in perovskite with each grain size.

crystals in most of silicates (Muehlenbachs and Kushiro, 1975; Jaoul *et al.*, 1981, 1983; Houlier *et al.*, 1988; Fisler *et al.*, 1997). It is obvious that diffusion of cation is almost always much faster than other ions in oxide and silicate minerals. Gaustason and Muehlenbachs (1993) calculated oxygen diffusion rates in $(Mg,Fe)SiO_3$ perovskite from the anion porosity Φ defined as $1-V_A/V$, where V_A is the volume of anions in the unit cell and V is the unit cell volume, to be $\ln D = A + B\Phi - (L+M\Phi) / RT$, where $A = 36.5\pm7.7$, $B = -1.01\pm0.17$, $L = 1116\pm60$ and $M = -18.6\pm1.3$, and $\Phi \approx 15\%$ at 25 GPa (fig. 4-8). If their calculation is correct, the diffusion coefficient of oxygen is about several order of magnitude larger than that of silicon in the wide range of temperature (fig. 4-8), and silicon diffusion ultimately controls the effective diffusion in perovskite (fig. 4-9). At lower temperature (< 1100~1200 °C), however, oxygen diffusion may control the effective diffusion (fig. 4-9).

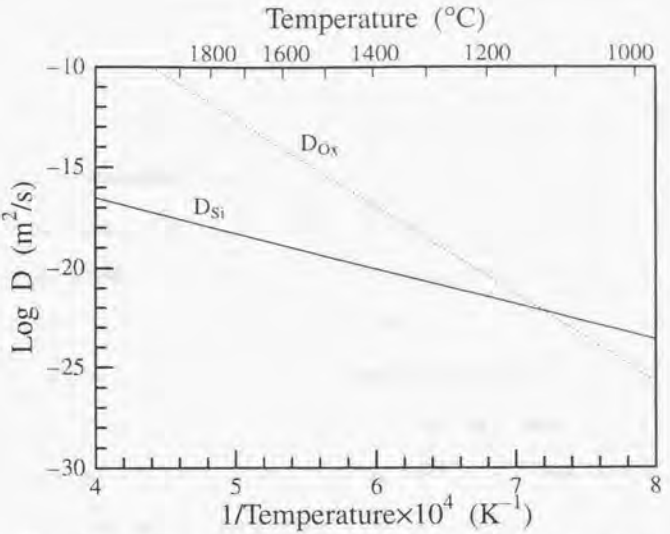

Fig. 4-8. Silicon self-diffusion coefficient in perovskite lattice determined in this study (solid line) and oxygen self-diffusion coefficient calculated by Gautason and Muehlenbaches (1993) (dotted line).

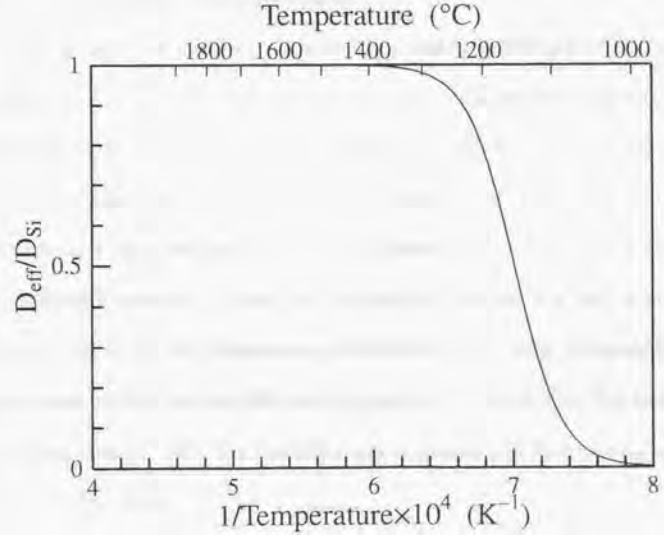

Fig. 4-9. The ratio of silicon diffusion (D_{Si}) and effective diffusion (D_{eff}), which was estimated by the relation of eqn. 4.4, as a function of temperature, assuming that diffusion is controlled by lattice. The D_{Si} is dominant mechanism in bulk diffusion at higher temperature (≥ 1200°C).

5. Geophysical implications

Deformation in the lower mantle

The textures of perovskite and periclase (magnesiowüstite) aggregates in the previous study (Ito and Sato, 1991) and in the present study (fig. 3-2) show that perovskite grains tend to form a network whereas periclase grains tend to round and isolate. It is unlikely that rheological properties of the lower mantle is determined by those of magnesiowüstite suggested by Karato (1980), because magnesiowüstite does not form continuous films along grain boundaries of perovskite. Consequently, it is concluded that deformation in the lower mantle, which composes of perovskite exceeding 85 % of its volume (Stixrude et al., 1992), depend on rheology of perovskite because of a network of the perovskite grains.

According to the previous results by Karato and Li (1992) and Li *et al.* (1996), the dominant deformation mechanism in $CaTiO_3$ perovskite may be diffusion creep at lower mantle T/T_m (= 0.6-0.8) when the average grain size is less than millimeter orders (fig. 5-1 after Karato and Li, 1992). Assuming that their result is applicable to $MgSiO_3$ perovskite, it is likely that diffusion creep is dominant deformation mechanism rather than dislocation creep in the lower mantle when the average grain size is less than millimeter orders. For the diffusion creep, the effective viscosity is independent of the applied stress and therefore the flow can be regarded as Newtonian fluid (Raj and Ashby, 1971; Karato and Li, 1992). The viscosity η can be described by the following equation (Raj and Ashby, 1971)

$$\frac{1}{\eta} = A\frac{\Omega}{RT}\frac{D_{eff}}{G^2} \qquad (5.1)$$

where A is constant (≈13.3) and Ω is mole volume, where Ω is ≈2.44×10^{-5} m^3/mol for perovskite at 1 atm (Horiuchi *et al.*, 1987). There is little pressure effect on the mole volume why the V/V_0 is less than 0.9 at around 25 GPa, where V_0 is the unit cell volume at 1 atm and V is the unit cell volume at high pressure and high temperature (Funamori *et al.*, 1996). The relation between temperature-viscosity-grain size was estimated in fig. 5-2. The boundary between diffusion and dislocation creep is assumed by the extrapolating of Karatos' results (fig. 5-1). The viscosity of the upper portions of the regular lower mantle has been inferred to be 10^{21}-10^{23} Pa·s by means of analyses of the post-glacial rebound (Nakada and Lambeck, 1989; Mitrovica and Peltier, 1991; Lambeck *et al.*, 1996), and temperature at the uppermost lower mantle is estimated to be 1873±100 K (Ito and Katsura, 1989). Therefore, the grain size of perovskite in the regular lower mantle around 700 km depth is estimated to be 1-10 mm in similar to that of olivine in the upper mantle rocks (Ave Lallemant et al. (1980) measured the grain size of olivine of mantle xenoliths to be 1-13 mm).

Considering that temperature in the lower mantle is estimated to be more than 1873 K (*e.g.* Jeanloz and Morris, 1986), the effective diffusion in the lower mantle may be almost represented by lattice diffusion but not grain boundary diffusion if the grain size is larger than a few tens micrometers (fig. 4-7). Therefore, the dominant deformation mechanism in the large part of the lower mantle seems to be the lattice diffusion creep without any correction of pressure effects, where the effective viscosity is proportional to the square of the grain size (eqns. 4.2 and 5.1), controlled by silicon

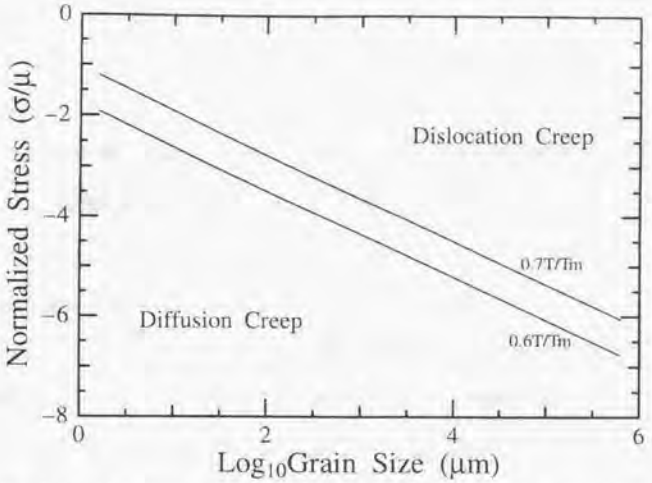

Fig. 5-1. Deformation mechanism map for $CaTiO_3$ perovskite. Solid lines are the boundaries between dislocation and diffusion creep for orthorhombic structure at T/T_m = 0.6 and 0.7. The range of stress expected in the lower mantle is 1-10 MPa (normalized stress $\sigma/\mu = 10^{-4}$ to 10^{-5}). Modified after Karato and Li (1992).

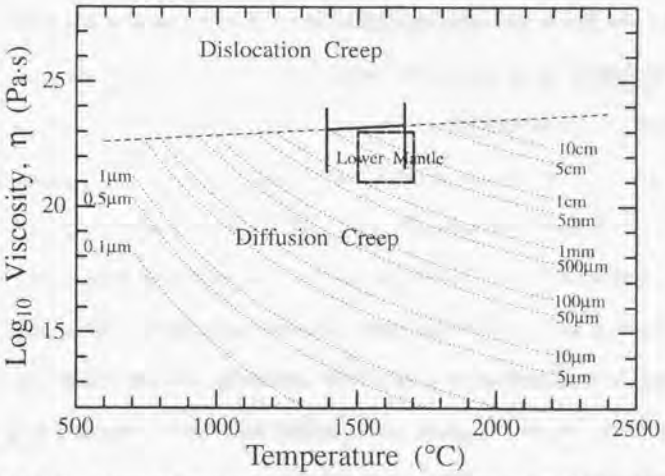

Fig. 5-2. Temperature-viscosity relations with each grain size (0.1 μm to 10 cm), represented by dotted lines. The range of temperature and viscosity in the lower mantle are considered to be 1600 ± 100 °C at around 670 km depth (Ito and Katsura, 1989) and 10^{21}-10^{23} Pa·sec (*e.g.* Lambeck *et al.*, 1996). The boundary, showed by solid and dashed lines, between diffusion creep and dislocation creep was assumed by extrapolating of Karatos' results (fig. 5-1).

diffusion in perovskite because of the lower diffusivity of silicon than that of oxygen in perovskite (section 4.3) with grain size of 1-10 mm (fig. 5-2).

Rheology of the subducting slab

Some seismic tomographic studies reveal that the high-velocity zone, which may correspond to a cold subducted slab, penetrates into the lower mantle and continues even to the core-mantle boundary (Van der Hilst *et al.*, 1991, 1997). The subducting slab, mainly composed of olivine, underwent once or twice transformations before attaining the lower mantle. Along the mantle geotherm, at 400 km depth olivine (α phase) transforms to modified spinel (β phase) and at 550 km depth modified spinel (β phase) transforms to spinel (γ phase). On the other hand, in the case of cold slab, olivine transformed directly into spinel because of metastable α phase in the stable field of β phase due to low temperature < 600°C (Suito, 1977). The mechanism of olivine to spinel transition reported to be martinstic and coherent, and it causes the topotactic relation between olivine and spinel (Poirier, 1981). The preferred orientation of olivine in the upper mantle have been inferred from the seismic anisotropy (Anderson and Dziewonski, 1984; Tanimoto and Anderson, 1984) and from preferred orientation of olivine in xenoliths (Mercier and Nicolas, 1974). The preferred orientation changes the rheological properties of bulk rocks because of the change in dominant slip systems. The differential stress in the lower mantle has been estimated to be ~10MPa based on the relation $\dot{\varepsilon} = \sigma/\eta$, where the strain rate $\dot{\varepsilon}$ is assumed to be 10^{-15} sec from the velocity of plates and depth of the lower mantle (Karato and Li, 1992) and viscosity in the lower

mantle η is assumed to be 10^{21}-10^{23} Pa·s (Nakada and Lambeck, 1989; Mitrovica and Peltier, 1991; Lambeck *et al.*, 1996). Because the transformation from spinel to post-spinel should be the incoherent nucleation and growth mechanism under low differential stress (section 4.1) (Fujino and Irifune, 1992), there is no preferred orientation in the subducting slab transformed from spinel to post-spinel.

When a subducting slab passes through the 670 km discontinuity, a significant grain size reduction should occur in the subducted slab because of phase transformation from spinel to perovskite and magnesiowüstite (Ito and Sato, 1991). Ito and Sato (1991) reported that $(Mg,Fe)SiO_3$ perovskite and (Mg,Fe)O magnesiowüstite assemblage formed after 1 hour at 1600°C and 24 GPa was an aggregate of grains 0.1-2.0 μm in size. In the present study, it was observed that the significant grain size reduction was caused by the transformation from Mg_2SiO_4 spinel to $MgSiO_3$ perovskite and periclase (fig. 3-2). The expected grain size reduction in the subducted slab affects on its rheology, according to eqn. 5.1. The strength of subducted slab suddenly soften at the 670 km discontinuity, as well as softening at 400 km discontinuity due to α-β transition (Rubie, 1984). The grains of perovskite and magnesiowüstite start to grow after spinel-post spinel transformation. From the relation between grain size and viscosity (eqn. 5.1), rheological properties of the transformed slab depend strongly on grain growth rates. Grain size change with time after transformation was estimated by extrapolating the experimental results as eqns. 3.5, 3.6 and 3.7 (fig. 4-3). It has been pointed out that the initial grain size of transformed phase by the mechanism of nucleation and growth depends on the nucleation rate and growth rate during transformation (Riedel and

Karato, 1996, 1997). The initial grain size can not be estimated here because a lack of kinetic date for transformation from spinel to post-spinel. However, when the initial grain size is smaller than a few micrometers, the initial grain size little affects on the grain size after growth for geological time scale because of high growth rate with small grain sizes and low growth rate with large grain sizes. The change in viscosity of the subducted slab as a function of time after the transformation is calculated from eqns. 3.5, 3.7 and 5.1 (fig. 5-3), assuming that the diffusion in perovskite is controlled by silicon, due to a lack of the data for grain boundary diffusion of oxygen in perovskite, with initial grain size of less than a few micrometers. It is considered that grain growth of lower mantle rocks is represented by the dual phase growth rather than single phase growth. As shown in fig. 5-3, it is notable that the viscosity curves show slightly convex, suggesting that dominant diffusion mechanism is changed from the grain boundary diffusion to the lattice diffusion. If the subduction rate is 10 cm/year, it takes ~1 My for the slab to reach the depth of 700 km from 670 km after transformation. Although the transformed slab may be cooler about several hundreds degrees than the surrounding mantle at the depth of 700 km (Schubert *et al.*, 1975) (fig. 5-4), it is concluded that the viscosity of subducted slab is 10^{17}-10^{19} Pa·s and it is about 4 order of magnitude lower than that of the surrounding mantle.

The subducting slab has the thermal structure such as the central core in the slab is cooler than the edge portion of slab (Schubert *et al.*, 1975) (fig. 5-4). Such thermal structure in the subducted slab causes the rheologically layered structure. Fig. 5-5 shows the variation of viscosity as a function of distance from the slab-regular mantle interface.

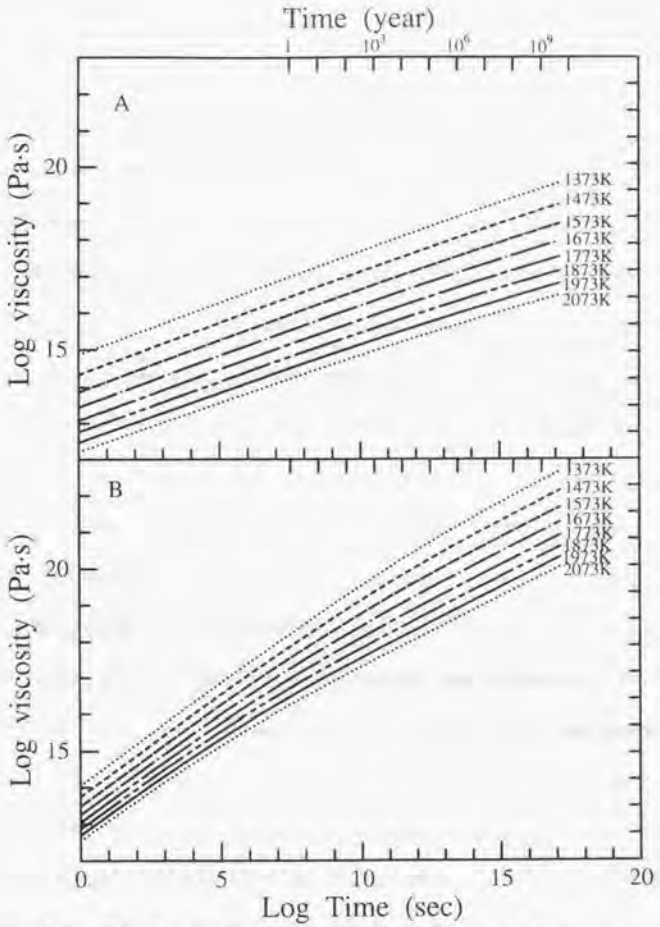

Fig. 5-3. The change of viscosity of subducted slab into the lower mantle with time at constant temperature, without the consideration of initial grain size. "Time" means the duration for grain growth of perovskite after transformation from spinel to perovskite and periclase. (A) The grain growth rate of perovskite in dual phase was used (eqn. 3.5), and (B) growth rate of perovskite in single phase was used (eqn. 3.7). Note that the lines representing viscosity are slightly bending, suggesting that dominant diffusion mechanism is changed from grain boundary diffusion to lattice diffusion. The viscosity of the lower mantle is 10^{21}-10^{23} Pa·sec based on the observation of post-glacial rebound (*e.g.* Lambeck et al., 1996).

The viscosity is estimated to be 10^{18}-10^{20} Pa·s at the center of slab (η_{center}), 10^{16}-10^{18} Pa·s at the edge of slab (η_{edge}) and 10^{21}-10^{23} Pa·s in the surrounding mantle (η_{mantle}) (Nakada and Lambeck, 1989; Mitrovica and Peltier, 1991; Lambeck *et al.*, 1996), that is, $\eta_{center} < \eta_{edge} < \eta_{mantle}$. Here, the subducting slab includes the basaltic layer which transformed into a hard garnetite layer (Irifune and Ringwood, 1993; Karato *et al.*, 1995b). However, the thickness of garnetite layer is 5-10 km smaller than that of lithosphere, and Karato (1997) suggested the separation of the garnetite layer from subducting lithosphere during passing though the 670 km discontinuity. Therefore, it is likely the rheological structure without garnetite layer in the lower mantle as shown in fig. 5-5. This rheological structure may affect the dynamics of the subducting slab into the deeper lower mantle because such thermal structure may be kept during sinking of subducted slab to core mantle boundary on the evidence of seismic tomography (Van der Hilst et al., 1997). However it have been reported that subducted slab which transformed from olivine to spinel at low temperature has smaller grain size than that transformed at high temperature (Riedel and Karato, 1997), since it is necessary to know the initial grain size for understanding the correct rheological structure.

Many experimental observations (*e.g.*, Funamori and Yagi, 1993) and theoretical modelings (Stixrude and Cohen, 1993) suggest no structure transformation from orthorhombic to tetragonal structure in $(Mg,Fe)SiO_3$ perovskite. In the present study, perovskite have been observed to be orthorhombic structure. However, some laboratory data (Wang *et al.*, 1991, 1992) suggested a structural phase transformation in

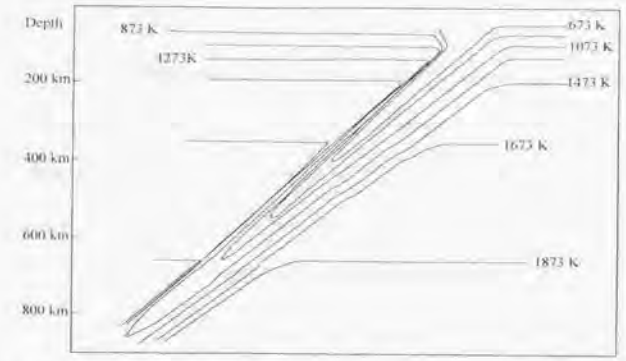

Fig. 5-4. Temperature in the subducting slab for dip angle of 45° and a constant subduction rate of 8 cm/y. The distributions of temperature are obtained by the calculations of Schubert *et al.* (1975) using mantle geotherm. Modified after Ito and Sato (1992).

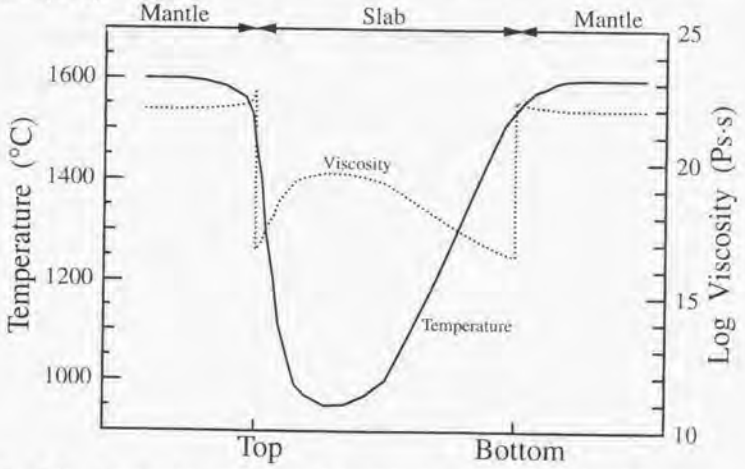

Fig. 5-5. Rheological structure in the subducting slab at around 700 km depth. "Top" and "Bottom" represent the boundaries between subducted slab and surrounding mantle. Dotted and solid line show the change of viscosity and temperature, which correspond with the distribution of temperature in fig. 5-4, respectively. It is assumed that the grain size in the surrounding mantle is 5 mm (fig. 5-2), and that the perovskite grains in the transformed subducting slab grow for 1 My (see section 5) at constant temperatures (eqn. 3.5, fig. 4-4A).

$(Mg,Fe)SiO_3$ perovskite in the lower mantle. Recently, seismological analysis indicated a discontinuity at around 920 km depth (Kawakatsu and Niu, 1994), which might correspond to a structural transformation in perovskite that changes elastic wave velocities (Fischer *et al.*, 1993). If the structural transformation is exist, rheological properties change corresponding to this structural transformation.

Rheological properties of perovskite are influenced by constituent minor elements. The iron content of 10 mol % in olivine makes the silicon diffusivity to be slow (fig. 4-4). Recently, it have been reported the large solubility of aluminum in perovskite (Miyajima *et al.*, 1997). It will be important for understanding rheology of the lower mantle to take into account not only iron content but also Al content in perovskite in future study.

6. Conclusion

In the present study, the TEM investigation revealed the no topotactic relation between Mg_2SiO_4 spinel and periclase and the transformation mechanism from Mg_2SiO_4 spinel to $MgSiO_3$ perovskite and periclase to be incoherent nucleation and growth.

The grain growth rate of perovskite and periclase in dual phase in its aggregates were determined to be for perovskite as,

$$G^{10.6\pm1.0} = 10^{57.4\pm5.9} t\exp\{-(320.8\pm33.9)/RT\}$$

and for periclase as,

$$G^{10.8\pm1.9} = 10^{62.3\pm11.6} t\exp\{-(247.0\pm55.3)/RT\}$$

where G is grain size in meter at time t in second, R is gas constant and T is absolute temperature, with activation energy in kJ/mol. The growth rate of perovskite at constant temperature of 1873 K in the single phase was determined to be

$$G^{5.3} = 10^{33.7} t$$

where G is grain size in meter at time t in second.

The self-diffusion coefficients of silicon in perovskite were determined to be

$$D_l = 4.12\left(^{+47.7}_{-3.79}\right)\times10^{-10}\exp\left\{-(341\pm40)/RT\right\}$$

$$\delta D_{gb} = 1.88\left(^{+18.9}_{-1.71}\right)\times10^{-16}\exp\left\{-(310\pm37)/RT\right\}$$

where D_l and D_{gb} are lattice diffusion coefficient in m^2/sec and grain boundary coefficient, respectively, and δ is the width of grain boundary.

The rheological properties determined in this study indicate follows; (1) The grain size of perovskite in the lower mantle is estimated to be 1-10 mm, which suggests that

lattice diffusion creep is dominant deformation mechanism in the large part of lower mantle; (2) The viscosity of subducted slab depends on the grain growth and is about 4 order of magnitude lower than that of the surrounding mantle at 700 km depth; (3) The thermal structure of the subducted slab results in the layered rheological structure of the subducted slab.

Acknowledgments

I am grateful to M. Toriumi, T. Kato, H. Yurimoto, and E. Ohtani for their helpful discussions and significant supports. I would like to thank K. Onuma and T. Fujii for the use of the high-pressure apparatus and useful comments, S. Karato for useful suggestions and critical comments, and A. Yasuda, A. Suzuki, T. Kubo, K. Mibe and H. Mizobata for the support for high pressure experiments. I am indebted to K. Fujino, N. Miyajima, N. Tomioka and T. Shinmei for the TEM investigation, and H. Yoshida for the SEM observation and EPMA analysis. I also thank H. Horiuchi for the use of the micro-area X-ray diffractometer, T. Kondo for the support for using of DAC and T. Yagi and M. Ozima for the providing enstatite single crystal, H. Nagahara for the providing forsterite single crystal, I. Miyagi for quantitative analysis of H_2O by using SIMS, S. Nakashima, I. Shimizu, H. Morishima, S. Ono, N. Shigematsu and T. Yoshino for helpful suggestions, M. Yutani for the use of the depth profiler and M. Ito for technical advice of coating of a ^{29}Si-enriched thin film.

References

Anderson, D. L. (1989) Composition of the earth, *Science* **243**, 367-370.

Anderson, D. L. and Dziewonski, A. M. (1984) Seismic tomography, *Sci. Am.* **251**, 58-66.

Atkinson, A. and Taylor, R. I. (1979) The diffusion of Ni in bulk and along dislocation in NiO single crystals, *Philos. Mag.* **A39**, 581-595.

Ave Lallemant, H. G., Mercier, J-C. C., Carter, N. L. and Ross, J. V. (1980) Rheology of the upper mantle: inferences from peridotite xenoliths, *Tectonophysics* **70**, 85-113 .

Baldo, J. B. and Bradt, R. C. (1988) Grain growth of lime and periclase phases in a synthetic doloma, *J. Am. Ceram. Soc.* **71**, 720-725.

Bass, J. D. (1984) Elasticity of single-crystal $SmAlO_3$, $GdAlO_3$ and $ScAlO_3$ perovskites, *Phys. Earth Planet. Inter.* **36**, 145-156.

Beauchesne, S. and Poirier, J. P. (1989) Creep of barium titanate perovskite: a contribution to a systematic approach to the viscosity of the lower mantle, *Phys. Earth Planet. Inter.* **55**, 187-199.

Béjina, F. and Jaoul, O. (1996) Silicon self-diffusion in quartz and diopside measured by nuclear micro-analysis methods, *Phys. Earth Planet. Inter.* **97**, 145-162.

Brook, R. J. (1976) Controlled grain growth, in *Treatise on Materials Science and Technology*, Vol. 9, Ceramic Fabrication Process, F. F. Wang, Ed. (Academic Press, New York, 1976), pp.331-364

Burke, J. E. (1949) The fundamentals of recrystallization and grain growth, in *Grain Control in Industrial Metallurgy*, (American Society for Metals, Cleveland, 1949), pp.1-73.

Carlson, W. D. and Rosenfeld, J. L. (1981) Optical determination of topotactic aragonite-calcite growth kinetics: metamorphic implications, *J. Geol.* **89**, 615-638.

Carpenter, R. W. (1967) Growth of modurated structure in gold-platinum alloys, *Acta Met.* **15**, 1567-1572.

Chen, I-W. and Xue, L. A. (1990) Development of superplastic structural ceramics, *J. Am. Ceram. Soc.* **73**, 2585-2609.

Clank, J. (1975) *The Mathematics of Diffusion, second edition*, Clarendon Press, Oxford, 1-414.

Dziewonski, A. M. and Anderson, D. L. (1981) Pleliminary reference earth model, *Phys. Earth Planet. Inter.* **25**, 297-356.

Fischer, G. J., Wang, Z. and Karato, S. (1993) Elasticity of $CaTiO_3$, $SrTiO_3$ and $BaTiO_3$ perovskite up to 3.0 GPa: the effect of crystallographic structure, *Phys. Chem. Mineral.* **20**, 97-103.

Fischer, K. M., Jordan, T. H. and Creager, K. C. (1988) Seismic constraints on the morphology of deep slabs, *J. Geophys. Res.*, **93**, 4773-4783.

Fisler, D. K., Mackwell, S. J. and Petsch, S. (1997) Grain boundary diffusion in enstatite, *Phys. Chem. Minerals* **24**, 264-273.

Fournelle, R. A. and Clark, J. B. (1972) The genesis of the cellular precipitation reaction, *Metall. Trans.* **3**, 2757-2767.

Fujino, K. and Irifune, T. (1992) TEM studies on the olivine to modified spinel transformation in Mg_2SiO_4, in *High-Pressure Research in Mineral Physics*, Y. Syono and M. H. Manghnani, Eds. (*Geophys. Monograph* American Geophysical Union, Washington, DC), pp. 237-243.

Fukao, Y., Obayashi, M., Inoue, M. and Nenbai, M. (1992) Subducting slabs stagnant in the mantle transition zone, *J. Geophys. Res.* **97**, 4809-4822.

Funamori, N. and Yagi, T. (1993) High pressure and high temperature in situ X-ray observation of $MgSiO_3$ perovskite under lower mantle conditions, *Geophys. Res. Lett.* **20**, 387-390.

Funamori, N., Yagi, T., Utsumi, W., Kondo, T., Uchida, T. and Funamori, M. (1996) Thermoelastic properties of $MgSiO_3$ perovskite determined by in situ X ray observation up to 30 GPa and 2000 K, *J. Geophys. Res.* **101**, 8257-8269.

Gautason, B. and Muehlenbachs, K. (1993) Oxygen diffusion in perovskite: Implications for electrical conductivity in the lower mantle, *Science* **260**, 518-521.

Glaeser, A. M. (1984) Microstructural developments in ceramics - The role of grain growth, *J. Ceram. Soc Japan* **92**, 538-546.

Gupta, T. K. (1971) Kinetics and mechanisms of pore growth in MgO, *J. Materials Sci.* **6**, 989-997.

Handy, M. R. (1994) Flow laws for rocks containing two nonlinear viscos phases: a phenomenological approch, *J. Struct. Geol.* **16**, 287-301.

Hanitzch, E. and Kalweit, M. (1968) The absorption of metal crystals from solution, *Z. Phys. Chem.* **57**, 145-152.

Harkulich, T. M., Magder, J, Vukasovich, M. S. and Lockhart, R. J. (1966) Ferroelectrics of ultrafine particle size: II, Grain growth inhibition studies, *J. Am. Ceram. Soc.* **49**, 295-299.

Harrison, L. G. (1961) Influence of dislocations on diffusion kinetics in solids with particular reference to the alkali halides, *Trans. Faraday Soc.* **57**, 1191-1199.

Hillert, M. (1965) On the theory of normal and abnomal grain growth, *Acta Metall.* **13**, 227-239.

Horiuchi, H., Ito, E. and Weidner, D. J. (1987) Perovskite-type $MgSiO_3$: Single-crystal X-ray diffraction study, *American Mineralogist* **72**, 357-360.

Hornbogen, E. (1972) Systematics of the celluar precipitation reaction, *Metall. Trans.* **3**, 2717-2727.

Hoshikuma, A., Sato, H. and Ito, E. (1995) Grain growth of the dissociation product of Mn2TiO4 spinel: Implications for superplasticity, *J. Seismol. Soc. Japan* **48**, 159-165.

Houlier, B., Jaoul, O., Abel, F. and Liebermann, R. C. (1988) Oxygen and silicon self-diffusion in natural olivine at T=1300°C, *Phys. Earth Planet. Inter.* **50**, 240-250.

Houlier, B., Cheraghmakani, M. and Jaoul, O. (1990) Silicon diffusion in San Carlos olivine, *Phys. Earth Planet. Inter.* **62**, 329-340.

Irifune, T. and Ringwood, A. E. (1993) Phase transformations in subducted oceanic crust and buoyancy relationships at depths of 600-800 km in the mantle, *Earth Planet. Sci. Lett.* **117**, 101-110.

Ito, E. and Takahashi, E. (1987) Ultrahigh-pressure phase transformations and the constitution of the deep mantle, in *High-Pressure Research in Mineral Physics*, S.

AAkimoto and M. H. Manghnani Eds. Center for Academic Publications, Tokyo, pp. 221-229.

Ito, E. and Katsura, T. (1989) A temperature profile of the mantle transition zone, *Geophys. Res. Lett.* **16**, 425-428.

Ito, E. and Takahashi, E. (1989) Postspinel transformations in the system Mg_2SiO_4-Fe_2SiO_4 and some geophysical implications, *J. Geophys. Res.* **94**, 10637-10646.

Ito, E and Sato, H. (1991) Aseismicity in the lower mantle by superplasticity of the descending slab, *Nature* **351**, 140-141.

Ito, E. and Katsura, T. (1992) Melting of ferromagnesian silicates under the lower mantle conditions, in *High-Pressure Research: Application to Earth and Planetary Sciences*, Y.Syono and M.H.Manghnani, Eds. (AGU, Washington, DC, 1992), pp315-322.

Ito, E. and Sato, H. (1992) Effect of phase transformations on the dynamics of the descending slab, in *High-Pressure Research in Mineral Physics*, Y. Syono and M. H. Manghnani, Eds. (*Geophys. Monograph* American Geophysical Union, Washington, DC), p. 257-262.

Jaoul, O. (1990) Multicomponent diffusion and creep in olivine, *J. Geophys. Res.* **95**, 17631-17642.

Jaoul, O., Poumellec, M., Froidevaux, C. & Havette, A. (1981) Silicon diffusion in forsterite: a new constraint for understanding mantle deformation, in *Anelasticity in the Earth*, edited by F.D.Stacey *et al.*, pp. 95-100. Godyn.Ser., vol 4. AGU, Washington, DC.

Jaoul, O., Houlier, B. and Abel, F. (1983) Study of ^{18}O diffusion in magnesium

orthosilicate by nuclear microanalysis, *J. Geophys. Res.* **88**, 613-624.

Jeanloz, R. and Morris, S. (1986) Temperature distribution in the crust and mantle, *Annu. Rev. Earth Planet. Sci.* **14**, 377-415.

Kapadia, C. M. and H.Leipold, M. (1974) Grain growth in pure dense MgO, *J. Am. Ceram. Soc.* **57**, 41-42.

Karato, S. (1981) Rheology of the lower mantle, *Phys. Earth Planet. Inter.* **24**, 1-14.

Karato, S. (1986) Rheology of synthetic olivine aggregates: Influence of grain size and water, *J. Geophys. Res.* **91**, 8151-8176.

Karato, S. (1988) The role of recrystallization in the preferred orientation of olivine, *Phys. Earth Planet. Inter.* **51**, 107-122.

Karato, S. (1989) Grain growth kinetics in olivine aggregates, *Tectonophysics* **168**, 255-273.

Karato, S. (1997) On the separation of crustal component from subducted oceanic lithosphere near the 660 km discontinuity, *Phys. Earth Planet. Inter.* **99**, 103-111.

Karato, S. and Li, P. (1992) Diffusion creep in perovskite: Implications for the rheology of the lower mantle, *Science* **255**, 1238-1240.

Karato, S., Zhang, S. and Wenk, H. R. (1995a) Superplasticity in earth's lower mantle: Evidence from seismic anisotropy and rock physics, *Science* **270**, 458-461.

Karato, S., Wang, Z., Liu, B. and Fujino, K. (1995b) Plastic deformation of garnets: systematics and the implications for the rheology of mantle transition zone, *Phys. Earth Planet. Inter.* **130**, 13-30.

Kato, T., Ohtani, E., Morishima, H., Yamazaki, D., Suzuki, A., Suto, M., Kubo, T., Kikegawa, T. and Shimomura, O. (1995) In situ X ray observation of high-

pressure phase transitions of $MgSiO_3$ and thermal expansion of $MgSiO_3$ perovskite at 25 GPa by double-stage multianvil system *J. Geophys. Res.* **100**, 20475-20481.

Kawakatsu, H. and Niu, F. (1994) Seismic evidence for a 920-km discontinuity in the mantle, **Nature 371**, 301-305.

Kennett, B. L. N. and Engdahl, E. R. (1991) Traveltimes for global earthquake location and phase identification, *Geophys. J. Int.* **105**, 429-465.

Kerschhofer, L., Sharp, T. G. and Rubie, D. C. (1996) Intracrystalline transformation of olivine to wadsleyite and ringwoodite under subduction zone conditions, *Science* **274**, 79-81.

Knittle, E. and Jeanloz, R. (1987) Synthesis and equation of state $(Mg,Fe)SiO_3$ perovskite to over 100 gigapascals, *Science* **235**, 668-670.

Kohlstedt, D. L., Goetze, C. and Durham, W. B. (1976) Experimental deformation of single crystal olivine with application to flow in the mantle, in *The Physics and Chemistry of Minerals and Rocks*, R. G. J. Strens, ed., John Wiley, New York, pp. 35-49.

Kumazawa, M. and Anderson, D. L. (1969) Elastic moduli, pressure derivatives, and temperature derivatives of single-crystal olivine and single-crystal forsterite, *J. Geophys. Res.* **74**, 5961-5972.

Lambeck, K., Johnston, P., Smither, C. and Nakada, M. (1996) Glacial rebound of the British Isles-III. Constraints on the mantle viscosity, *Geophys. J. Int.* **125**, 340-354.

Le Claire, A. D. (1963) The analysis of grain boundary diffusion measurements, *J. Appl.*

Phys. **14**, 351-356.

Li, P., Karato, S. and Wang, Z. (1996) High-temperature creep in fine-grained polycrystalline $CaTiO_3$, an analogue material of $(Mg,Fe)SiO_3$ perovskite, *Phys.Earth Planet. Inter.* **95**, 19-36 .

Lifshits, I. M. and Slyozov, V. V. (1961) The kinetics of precipitation from supersaturated solid solutions, *J. Phys. Chem. Solids* **19**, 35-50.

Mao, H. K., Chen, L., Hemley, R. J., Jephcoat, A. P. and Wu, Y. (1989) Stability and equation of state of $CaSiO_3$ perovskite to 134 GPa, *J. Geophys. Res.* **94**, 17889-17894.

Martinez, I., Wang, Y., Guyot, F., Liebermann, R. C. and Doukhan, J. C. (1997) Microstructures and iron partitioning in $(Mg,Fe)SiO_3$ perovskite-(Mg,Fe)O magnesiowüstite assemblages: an analytical transmission electron microscopy study, *J. Geophys. Res.* **102**, 5265-5280.

Meade, C., Silver, P. G. and Kaneshima, S. (1995) Laboratory and seismological observations of lower mantle isotropy, *Geophys. Res. Lett.* **22**, 1293-1296.

Mendelson, M. I. (1969) Average grain size in polycrystalline ceramics, *J. Am. Ceram. Soc.* **52**, 443-446.

Mercier, J-C. C. and Nicolas, A. (1974) Textures and fabrics of upper-mantle peridotites as illustrated by xenoliths from basalts, *J. Petrol.* **16**, 454-487.

Mitrovica, J. X. and Peltier, W. R. (1991) A complete formalism for the inversion of post-glacial rebound data: resolving power analysis, *Geophys. J. Int.* **194**, 267-288.

Miyajima, N., Fujino, K., Funamori, N., O'Neill, B., Kondo, T. and Yagi, T. (1997) Post-garnet phases in the lower mantle, *Special Issue of The Review of High Pressure Science and Technology, vol. 6 Joint conference: AIRAPT-16 & HPCJ-38 abstract,* p.65.

Miyazaki, T., Seki, K., Doi, M. and Kozakai, T. (1986) Stability bifurcations in the coarsening of precipitates in elastically constrained system, *Mater. Sci. Eng.* **77**, 125-132.

Miyazaki, T and Doi, M. (1989) Shape bifurcations in the coarsening of precipitates in elastically constrained systems, *Mater. Sci. Eng.* A**110**, 175-185.

Muehlenbachs, K. and Kushiro, I. (1975) Measurements of oxygen diffusion in silicates, *EOS trans.* Am. Geophys. Union **56**, V14.

Nakada, M. and Lambeck, K. (1989) Late Pleistocene and Holocene sea-level change in the Australian region and mantle rheology, *Geophys. J. Int.* **96**, 495-517.

Nichols, F. A. (1966) Theory of grain growth in porous compacts, *J. Appl. Phys.* **37**, 4599-4602.

Nicholson, G. C. (1966) Grain growth in magnesium oxide containing iron oxide or titanium dioxide, *J. Am. Ceram. Soc.* **49**, 47-49.

Ohtani, E., Suzuki, A. and Kato, T. (1997) Flotation of olivine and diamond in mantle melt at high pressure: its implications for fractionation in the deep mantle and ultradeep origin of diamond, *High Pressure-Temperature Research: Properties of Earth and Planetary Materials, AGU Monograph series,* in press.

Oishi, Y. and Kingery, W. D. (1960) Oxygen diffusion in periclase crystals, *J. Chem. Phys.* **33**, 905-906.

Poe, B. T., McMillan, P. F., Rubie, D. C., Chakraborty, S., Yarger, J. and Diefenbacher, J. (1997) Silicon and oxygen self-diffusivities in silicate liquids measured to 15 gigapascals and 2800 kelvin, *Science* **276**, 1245-1248.

Poirier, J. P. (1981) On the kinetics of olivine-spinel transition, *Phys. Earth Planet. Inter.* **26**, 179-187.

Poirier, J. P. (1985) Creep of crystals, *Cambridge Earth Science Series, Cambridge University Press*, 1-260.

Poirier, J. P., Peyronneau, J., Gresland, J. Y. and Brebec, G. (1983) Viscosity and conductivity of the lower mantle: an experimental study on $MgSiO_3$ analogue, $KZnF_3$, *Phys. Earth Planet. Inter.* **32**, 273-287.

Poirier, J. P., Peyronneau, J., Madon, M., Guyot, F. and Revcolevschi, A. (1986) Eutectoid phase transformation of olivine and spinel into perovskite and rock salt structures, *Nature* **321**, 603-605.

Poirier, J. P., Beauchesne, S. and Guyot, F. (1989) Deformation mechanisms of crystals with perovskite structure, in *Perovskite: A Structure of Great Interest to Geophysics and Materials Science.* A Navrotsky and D. J. Weidner Eds. Am. Geophys. Union, Washington DC, pp. 119-123.

Puls, M. P. and Kirkaldy, J. S. (1972) The pearlite reaction, *Metall. Trans.* **3**, 2777-2796.

Raj, R. and Ashby, M. F. (1971) On grain boundary sliding and diffusional creep, *Metallugical Transactions* **2**, 1113-1127.

Riedel, M. R. and Karato, S. (1996) Microstructural development during nucleation and growth, *Geophys. J. Int.* **125**, 397-414.

Riedel, M. R. and Karato, S. (1997) Grain-size evolution in subducted oceanic lithosphere associated with the olivine-spinel transformation and its effects on rheology, *Earth Planet. Sci. Lett.* **148**, 27-43.

Ringwood, A. E. and Major, A. (1971) Synthesis of majorite and other high pressure garnets and perovskite, *Earth Planet. Sci. Lett.* **12**, 411-418.

Ringwood, A. E. (1991) Phase transformations and their bearing on the constitution and dynamics of the mantle, *Geochim. Cosmochim. Acta* **55**, 2083-2110.

Rubie, D. C. (1984) The olivine→spinel transformation and rheology of subducting lithosphere, *Nature* **308**, 505-508.

Rubie, D. C., Tsuchida, Y., Yagi, T., Utsumi, W., Kikegawa, T., Shimomura, O. and Brearley, A. J. (1990) An in situ X ray diffraction study of the kinetics of the Ni_2SiO_4 olivine-spinel transformation, *J. Geophys. Res.* **95**, 15829-15844.

Sakaguchi, I., Yurimoto, H. and Sueno, S. (1992) Self-diffusion along dislocations in single-crystal MgO, *Solid State Communications* **84**, 889-893.

Sakaguchi, I and Haneda, H. (1996) Oxygen tracer diffusion in single-crystal $CaTiO_3$, *J. Solid State Chem.* **124**, 195-197.

Saltykov, S. A. (1958) *Stereometric Metallography* (Metallurgizdat, Moscow) p.446

Schubert, G., Yuen, D. A. and Turcotte, D. L. (1975) Role of phase transitions in a dynamic mantle, *J. R. astr. Soc.* **42**, 705-735.

Senda, T. and Bradt, R. C. (1990) Grain growth in sintered ZnO and ZnO-Bi_2O_3 ceramics, *J. Am. Ceram. Soc.* **73**, 106-114.

Silver, P. G. and Chan, W. W. (1986) Observations of body wave multipathing from broadband seismograms: Evidence for lower mantle slab penetration beneath the Sea of Okhotsk, *J. Geophys. Res.* **91**, 13787-13802.

Stixrude, L., Hemly, R. J., Fei, Y. and Mao, H. K. (1992) Thermoelasticity of silicate perovskite and magnesiowüstite and stratification of the earth's mantle, *Science* **257**, 1099-1101.

Stixrude, N. and Cohen, R. E. (1993) Stability of orthorhombic $MgSiO_3$ perovskite in the Earth's lower mantle, *Nature* **364**, 613-616.

Suito, K. (1977) Phase relations of pure Mg2SiO4 up to 200 kilobars, in *High-Pressure Research in Mineral Physics*. M. H. Manghnani and S. Akimoto Eds. Academic Press, New York, pp. 225-266.

Tanimoto, T. and Anderson, D. L. (1984) Mapping convection in the mantle, *Geophys. Res. Lett.* **11**, 287-290.

Turnbull, D. and Hoffman, R. E. (1954) The effect of relative crystal and boundary orientations on grain boundary diffusion rates, *Acta Metall.* **2**, 419-426.

Turnbull, D. (1956) Phase changes, *Solid State Phys.* **3**, 225-306.

Van der Hilst, R., Engdahl, R., Spakman, W. and Nolet, G. (1991) Tomographic imaging of subducted lithosphere below northwest Pacific island arcs, *Nature* **353**, 37-43.

Van der Hilst, R. D., Widiyantoro, S. and Engdahl, E. R. (1997) Evidence for deep mantle circulation from global tomography, *Nature* **386**, 578-584.

Wagner, C. (1961) Theorie der alterung von niederschlagen durch umlosen, *Z. Elektrochemie* **65**, 581-591.

Wall, A. and Price, G. D. (1989) Defects and diffusion in $MgSiO_3$ perovskite: A computer simulation, in *Perovskite: A Structure of Great Interest to Geophysics and Meterials Science, Geophysical Monograph 45*, A. Navrotsky and D. J. Weidner Eds, AGU, Washington, D.C.

Wang, Y., Guyot, F., Yeganeh-Haeri, A. and Liebermann, R. C. (1990) Twinning in $MgSiO_3$ perovskite, *Science* **248**, 468-471.

Wang, Y., Weidner, D. J., Liebermann, R. C., Liu, X., Ko, J., Vaughn, M. T., Zhao, Y., Yeganeh-Haeri, A. and Pacalo, P. E. G. (1991) Phase transition and thermal expansion of $MgSiO_3$ perovskite, *Science* **251**, 410-413.

Wang, Y., Guyot, F. and Liebermann, R. C. (1992) Electron microscopy of (Mg,Fe)SiO3 perovskite: evidence for structural phase transformations and implications for the lower mantle, *J. Geophys. Res.* **97**, 12327-12347.

Wang, Y., Martinez, I., Guyot, F. and Liebermann, R. C. (1997) The breakdown of olivine to perovskite and magnesiowüstite, *Science* **275**, 510-513.

Wang, Z., Karato, S., and Fujino, K. (1993) High temperature creep of single crystal strontium titanate (SrTiO3): a contribution to creep systematics in perovskite, *Phys. Earth Planet. Inter.* **79**, 299-312.

Wong, J. (1980) Sintering and varistor characteristics of ZnO-Bi_2O_3 ceramics, *J. Appl. Phys.* **51**, 4453-4459.

Wright, K., Price, G. D. and Poirier, J. P. (1992) High-temperature creep of perovskites $CaTiO_3$ and $NaNbO_3$, *Phys. Earth Planet. Inter.* **74**, 9-22.

Wright, K. and Price, G. D. (1993) Computer simulation of defects and diffusion in perovskites, *J. Geophys. Res.* **98**, 22245-22253.

Yeganeh-Haeri, A., Weidner, D. J. and Ito, E. (1989) Elasticity of MgSiO3 in the perovskite structure, *Science* **243**, 787-789.

Yeganeh-Haeri, A. (1994) Synthesis and re-investigation of the elastic properties of single-crystal magnesium silicate perovskite, *Phys. Earth Planet. Inter.* **87**, 111-121.

Yoo, H-I., Wuensch, B. J. and Petuskey, W. T. (1985) Secondary ion mass spectrometric analysis of oxygen self-diffusion in single-crystal MgO, *Advance in Ceramics* **10**, 394-405.

Yurimoto, H. and Sueno, S. (1984) Anion and cation partitioning between olivine, plagioclase phenocrysts and the host magma: A new application of ion microprobe study, *Geochem.J.* **18**, 85-94.

Yurimoto, H., Morioka, M. and Nagasawa, H. (1992) Diffusion in single crystals of melilite: I. Oxygen, *Geochim. Cosmochim. Acta*, **53**, 2387-2394.

Yurimoto, H., Morioka, M. and Nagasawa, H. (1992) Oxygen self-diffusion along high diffusivity paths in forsterite, *Geochem. Jour.* **26**, 181-188.

Yusa, H., Akaogi, M. and Ito, E. (1993) Calorimetric study of $MgSiO_3$ garnet and pyroxene: heat capacities, transition enthalpies, and equilibrium phase relations in $MgSiO_3$ at high pressure and temperature, *J. Geophys. Res.* **98**, 6453-6460.

Zerr, A. and Boehler, R. (1994) Constraints on the melting temperature of the lower mantle from high-pressure experiments on MgO and magnesiowüstite, *Nature* **371**, 506-508.

Appendix Silicon self-diffusion in spinel

Mg_2SiO_4 spinel is dominant minerals in the mantle transition zone. To understand the rheological relation between the upper and lower mantle, silicon self-diffusion in spinel was preliminarily investigated.

High pressure experiment was carried out using malutianvil apparatus. The sample, which was composed of layered periclase in contact with layered enstatite, was pressurized up to 21 GPa and at 1600°C for annealing of 140 min (run no. IPG01). The spinel layer, which was formed by the reaction of periclase and enstatite, occurred on the boundary between periclase and enstatite (fig. A-1). The width of spinel layer was measured to be ~10 μm. Diffusion coefficient was determined to be $\sim 10^{-14}$ m^2/sec, calculating from the equation $x = (Dt)^{1/2}$ where x is the width of spinel layer after annealing of time t and D is diffusion coefficient (Fisler *et al.*, 1997).

Determined diffusion coefficient may represent the bulk (effective) diffusion of silicon in spinel (D^{sp}_{eff}). Therefore, because of $D^{sp}_{eff} > D^{pv}_{gb} > D^{pv}_{eff} > D^{pv}_{l}$ at 1873 K, silicon diffusion in Mg_2SiO_4 spinel may be faster than that in $MgSiO_3$ perovskite.

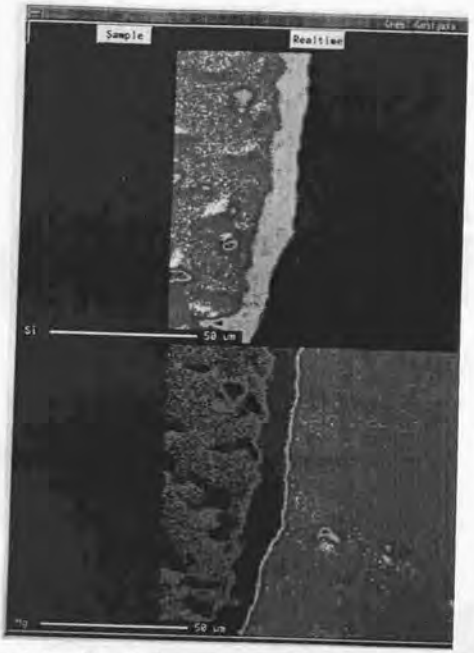

Fig. A-1. Chemical compositional mapping (upper, Si; lower, Mg) of run no. IPG01. Silicon and magnesium were measured using with an electron microprobe analyzer. Right, left and sandwiched portion represent periclase, ilmenite and spinel, respectively.

M. Torii '98

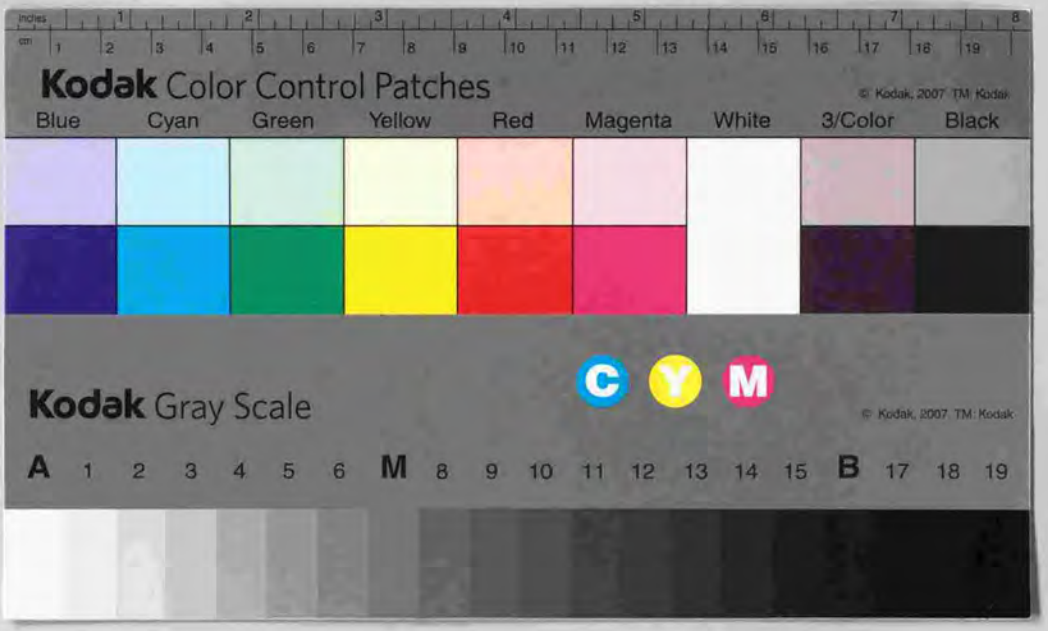
inches
cm
Kodak Color Control Patches
© Kodak, 2007 TM: Kodak
Blue
Cyan
Green
Yellow
Red
Magenta
White
3/Color
Black
C
Y
M
Kodak Gray Scale
© Kodak, 2007 TM: Kodak
A 1 2 3 4 5 6 M 8 9 10 11 12 13 14 15 B 17 18 19